ARTICLE

doi:10.1038/nature18590

Pore-forming activity and structural autoinhibition of the gasdermin family

Jingjin Ding[1,2], Kun Wang[2], Wang Liu[2], Yang She[1,2], Qi Sun[2], Jianjin Shi[2], Hanzi Sun[2], Da-Cheng Wang[1,3] & Feng Shao[1,2,4]

Inflammatory caspases cleave the gasdermin D (GSDMD) protein to trigger pyroptosis, a lytic form of cell death that is crucial for immune defences and diseases. GSDMD contains a functionally important gasdermin-N domain that is shared in the gasdermin family. The functional mechanism of action of gasdermin proteins is unknown. Here we show that the gasdermin-N domains of the gasdermin proteins GSDMD, GSDMA3 and GSDMA can bind membrane lipids, phosphoinositides and cardiolipin, and exhibit membrane-disrupting cytotoxicity in mammalian cells and artificially transformed bacteria. Gasdermin-N moved to the plasma membrane during pyroptosis. Purified gasdermin-N efficiently lysed phosphoinositide/cardiolipin-containing liposomes and formed pores on membranes made of artificial or natural phospholipid mixtures. Most gasdermin pores had an inner diameter of 10–14 nm and contained 16 symmetric protomers. The crystal structure of GSDMA3 showed an autoinhibited two-domain architecture that is conserved in the gasdermin family. Structure-guided mutagenesis demonstrated that the liposome-leakage and pore-forming activities of the gasdermin-N domain are required for pyroptosis. These findings reveal the mechanism for pyroptosis and provide insights into the roles of the gasdermin family in necrosis, immunity and diseases.

Pyroptosis is critical for host defences against infection and danger signals, and excessive pyroptosis causes immunological diseases and septic shock. Pyroptosis involves cell swelling and lysis, which causes massive release of cellular contents and thereby triggers strong inflammation[1]. The term pyroptosis was originally used to describe caspase-1-mediated macrophage death[2]. Caspase-1 belongs to the inflammatory caspase group, which also includes murine caspase-11 and its human counterparts caspase-4 and -5 (ref. 3). Unlike caspase-11 (ref. 4), caspase-4 and -5 can also activate pyroptosis in non-monocytotic cells[3]. Caspase-1 acts downstream of the inflammasome complex, which is scaffolded by an Nod-like receptor (NLR) protein, absent in melanoma 2 (AIM2) or pyrin, and recognizes bacteria, other microbes and endogenous threats[5,6]. Caspase-4, -5 and -11 sense[7,8] and are activated by direct binding to lipopolysaccharide (LPS)[3,9]; hyperactivation of these caspases causes septic shock.

Recent studies have identified the GSDMD protein, which critically determines pyroptosis[10,11]. GSDMD is cleaved by all inflammatory caspases between its N-terminal gasdermin-N and C-terminal gasdermin-C domains. This cleavage releases the autoinhibition by gasdermin-C of gasdermin-N, which has intrinsic pyroptosis-inducing activity. The absence of GSDMD does not affect caspase-1 processing of interleukin (IL)-1β, but blocks mature IL-1β secretion, suggesting that pyroptosis is required for noncanonical cytokine secretion[10,11]. Besides GSDMD, the gasdermin family also includes GSDMA, GSDMB, GSDMC, DFNA5 and DFNB59 (refs 12,13). Mice lack GSDMB but have three GSDMA (GSDMA1–3) and four GSDMC (GSDMC1–4) proteins. Other gasdermins are insensitive to inflammatory caspases[10]. Dominant mutations in *Gsdma3* (refs 14–16) and *DFNA5* (or autosomal recessive mutation in *DFNB59*)[17,18] cause alopecia and hyperkeratosis in mice and nonsyndromic hearing loss in humans, respectively. Disease-associated mutants of GSDMA3 and its gasdermin-N domain alone can activate pyroptosis owing to loss of autoinhibiton[10]. Despite the importance of gasdermins in pyroptosis and inflammation, the mechanisms of action of GSDMD and the gasdermin family are unknown.

Cytotoxicity of gasdermin-N from multiple gasdermins

All gasdermins, except for DFNB59, adopt a two-domain architecture. As found in GSDMD and GSDMA3 (ref. 10), the gasdermin-N domains of GSDMA, GSDMB, GSDMC or DFNA5, but not the full-length proteins, induced extensive pyroptosis in human 293T cells (Extended Data Fig. 1a, b). This suggests that gasdermins in general are pyroptosis factors. Expression of the GSDMD gasdermin-N domain (GSDMD-N) is highly toxic to *Escherichia coli* (Extended Data Fig. 1c, d), whereas little cytotoxicity was observed with full-length GSDMD and its GSDMD-C domain (both proteins could be highly expressed in *E. coli*). Similar phenomena were observed with GSDMA, GSDMA3, GSDMC and DFNA5 (Extended Data Fig. 1d). Thus, the gasdermin-N domain has intrinsic cytotoxicity in mammalian cells and its overexpression can also kill bacteria.

Gasdermin-N domains can bind membrane lipids

We hypothesized that the gasdermin-N domains might disrupt membranes to cause pyroptosis. To test this hypothesis, we assayed the binding of recombinant gasdermin-N to membrane lipids. To circumvent the toxicity of gasdermin-N in *E. coli*, a PreScission protease (PPase) site (LEVLFQGP) was engineered into the inter-domain linker in GSDMD, GSDMA and GSDMA3 (it has been shown that PPase cleavage of the engineered GSDMD or GSDMA3 can trigger pyroptosis[10]) and purified full-length gasdermins. Notably, the gasdermin-N and -C domains remained bound together following *in vitro* PPase cleavage. When the noncovalent complexes (N+C) were incubated with liposomes containing phosphatidylcholine as the skeleton lipid, all three gasdermin-N (30–35 kDa) but not gasdermin-C domains (20–25 kDa) were precipitated by liposomes containing 10% or 20% phosphatidylinositol-4,5-bisphosphate (PtdIns(4,5)P_2) (a major phosphoinositide in the plasma membrane), but not unphosphorylated phosphatidylinositol (Fig. 1a and Extended Data Fig. 2a, b). Neither full-length GSDMD, GSDMA and GSDMA3 nor their gasdermin-C domains bound phosphoinositide. Gasdermin-N could also bind to liposomes containing monophosphorylated (PtdIns3P, PtdIns4P and PtdIns5P),

[1]National Laboratory of Biomacromolecules, Institute of Biophysics, Chinese Academy of Sciences, Beijing, 100101, China. [2]National Institute of Biological Sciences, Beijing, 102206, China. [3]Foshan University, Guangdong, 528000, China. [4]National Institute of Biological Sciences, Collaborative Innovation Center for Cancer Medicine, Beijing, 102206, China.

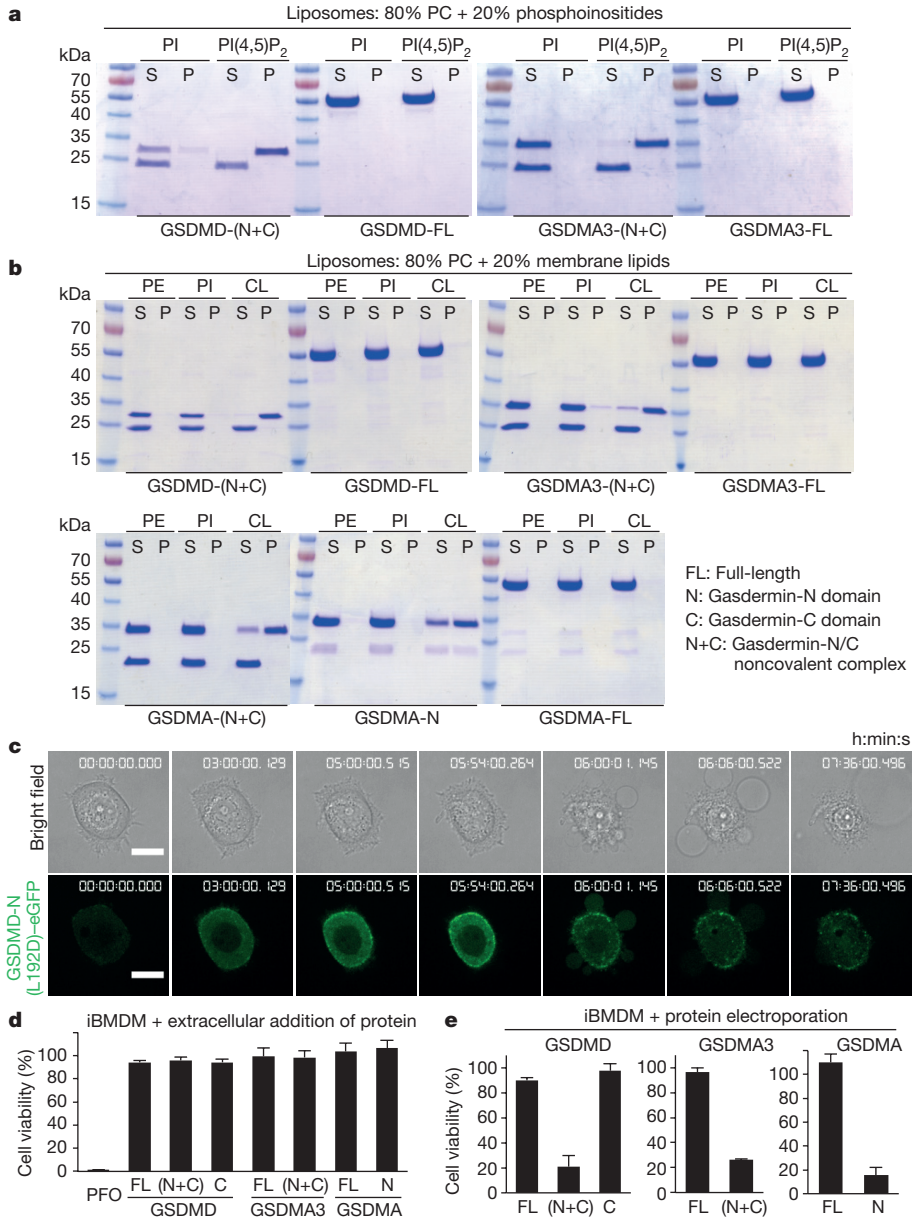

Figure 1 | Lipid binding, biomembrane association and disruption by the gasdermin-N domain. a, **b**, Binding of the gasdermin-N domain to membrane lipids. Purified gasdermin proteins were incubated with liposomes with indicated lipid compositions. After ultracentrifugation, the liposome-free supernatant (S) and the liposome pellet (P) were analysed by SDS–PAGE and Coomassie blue staining. CL, cardiolipin; PC, phosphatidylcholine; PE, phosphatidylethanolamine; PI, phosphatidylinositol. The gasdermin-N and -C noncovalent complex was obtained from inter-domain cleavage of the full-length (FL) protein. **c**, Microscopy imaging of GSDMD-N localization in cells during pyroptosis. GSDMD-N(L192D)–eGFP was stably expressed in HeLa cells under a tetracycline-inducible promoter. Shown are representative time-lapse cell images (brightfield and fluorescence) taken from 4–5 h after doxycycline addition. Scale bar, 15 μm. For videos of two representative cells, see Supplementary Videos 1 and 2. **d**, **e**, Effects of extracellular or intracellular delivery of purified gasdermin proteins on iBMDM cell viability. Equal amounts of indicated gasdermin proteins or PFO were added directly into cell culture medium (**d**) or electroporated into the cytosol (**e**). ATP-based cell viability is expressed as mean ± s.d. from three technical replicates. All data shown are representative of three independent experiments.

bisphosphorylated (PtdIns(3,4)P_2 and PtdIns(3,5)P_2) or triphosphophorylated (PtdIns(3,4,5)P_3) phosphatidylinositols (Extended Data Fig. 2b). Similar PtdIns(4,5)P_2 binding was observed with liposomes made of complicated phospholipid mixtures (phosphatidylcholine, phosphatidylethanolamine, phosphatidylserine, phosphatidylinositol and PtdIns(4,5)P_2) that mimic plasma membrane lipid composition (Extended Data Fig. 2c).

Cardiolipin and phosphatidylethanolamine are major bacterial membrane lipids. The gasdermin-N domains of GSDMD, GSDMA and GSDMA3, but not the full-length proteins or their gasdermin-C domains, were efficiently and specifically precipitated by cardiolipin liposomes (Fig. 1b). Reducing cardiolipin concentration from 20% to 10% decreased the binding efficiency (Fig. 1b and Extended Data Fig. 2d). Specific binding of gasdermin-N to cardiolipin, as well as the phosphoinositides, was also evident in the lipid-strip binding assay (Extended Data Fig. 2e). Thus, cardiolipin and phosphoinositide are two membrane lipid targets of gasdermin-N.

For the three gasdermins GSDMD, GSDMA and GSDMA3, only the gasdermin-N domain of GSDMA could be separated from the noncovalent complex by high-salt buffer. The apo-GSDMA-N domain showed similar binding to cardiolipin or phosphoinositide liposomes as the noncovalent complex (Fig. 1b and Extended Data Fig. 2a, c, d), suggesting that lipid binding by GSDMA does not involve gasdermin-C. Moreover, the three gasdermin-N domains bound strongly to cardiolipin liposomes; GSDMA-N showed weaker binding to phosphoinositide liposomes than GSDMD-N or GSDMA3-N despite their comparable pyroptosis-inducing activity (Extended Data Fig. 1a, b). A possible cause of this phenomenon is that artificial liposomes may not exactly recapitulate the complex lipid constituents of biomembranes.

Membrane targeting of gasdermin-N during pyroptosis

We next examined the localization of gasdermin-N during pyroptosis. Extracts of *Gsdmd*$^{-/-}$ immortalized bone marrow macrophages (iBMDMs) stably expressing Flag–GSDMD[10] were sequentially centrifuged (700*g*, 20,000*g* and 100,000*g*). Full-length GSDMD was found exclusively in the supernatant after 100,000*g* centrifugation (S100) (Extended Data Fig. 3a), suggesting a cytosolic localization. When pyroptosis was induced by LPS electroporation, GSDMD was cleaved into GSDMD-N and GSDMD-C; while GSDMD-C remained in S100, a large portion of GSDMD-N was distributed in the P7 heavy-membrane (pellet from 700*g* centrifugation) and P20 light-membrane fractions, which resembles the distribution of LAMP1 (endosome/lysosome),

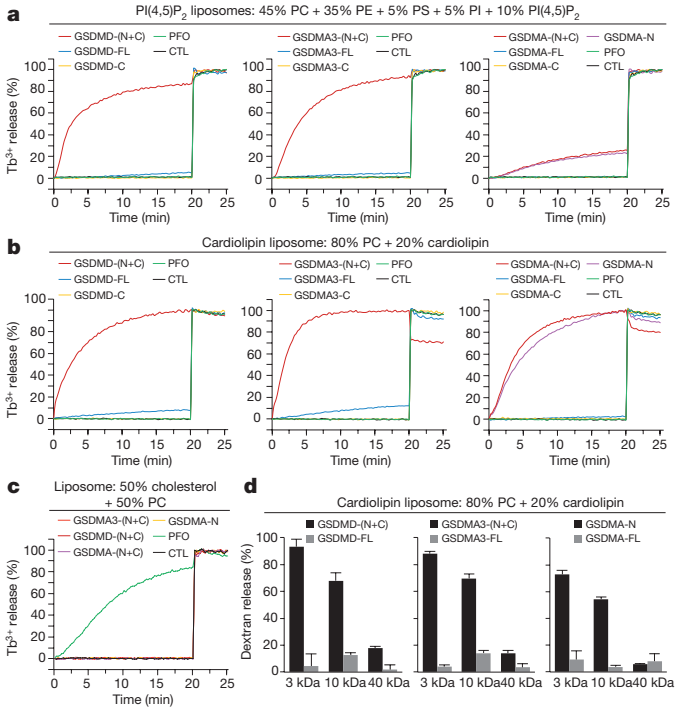

Figure 2 | Liposome-leakage-inducing activity of the gasdermin-N domain. Liposomes with indicated lipid compositions were treated with purified gasdermin proteins or PFO as indicated. **a–c**, Liposome leakage was monitored by measuring 2,6-pyridinedicarboxylic acid (DPA) chelating-induced fluorescence of released Tb^{3+}. Time course of relative Tb^{3+} release is shown. CTL, control. **d**, Different-size fluorescent dextrans were encapsulated into the liposome and the released dextran fluorescence was determined. Triton X-100 treatment was used to achieve 100% liposome leakage. Final leakage of the dextrans is expressed as mean ± s.d. from three technical replicates. All data shown are representative of three independent experiments.

Na, K-ATPase α1 (plasma membrane) and syntaxin 6 (*trans*-Golgi) (Extended Data Fig. 3a). GSDMD-N was also found in the lightest P100 fraction. As expected, actin and mitochondrial proteins (COX4 and TOM20) were found in the S100 and P7 fractions, respectively. The gasdermin-N domain of PPase-cleavable GSDMA showed the same distribution in pyroptotic 293T cells (Extended Data Fig. 3b). Thus, certain gasdermin-N domains moved to heterogeneous membranes during pyroptosis, echoing the binding to various phosphoinositides.

To visualize the membrane targeting, GSDMD-N and GSDMA3-N fused to enhanced green fluorescent protein (eGFP) were inducibly expressed in HeLa cells. The pyroptosis triggered by gasdermin-N expression was too severe and rapid to allow accumulation of fluorescence signals sufficient for detection. This was overcome by a mutation of leucine192 to aspartate (L192D), which slowed down the pyroptosis (see below). GSDMD-N(L192D) showed initial cytoplasmic distribution, and some of it was translocated and accumulated on the plasma membrane as pyroptosis progressed; the cells then developed characteristic swelling bubbles and became ruptured (Fig. 1c and Supplementary Videos 1, 2). Similar results were obtained with GSDMA3-N containing an equivalent L184D mutation (Extended Data Fig. 3c and Supplementary Videos 3, 4).

Biomembrane disruption correlates with lipid binding

Perfringolysin O (PFO) is a cholesterol-targeting pore-forming toxin from *Clostridium perfringens*. Extracellular addition of purified PFO to iBMDMs caused severe cytotoxicity (Fig. 1d). By contrast, the noncovalent complex of cleaved GSDMD or GSDMA3 or the GSDMA-N domain induced cell lysis only when delivered cytosolically but not when administered extracellularly (Fig. 1d, e). Identical results were obtained in 293T cells (Extended Data Fig. 3d, e). These findings are consistent with the presence of cholesterol in the exoplasmic leaflet of the plasma membrane and the localization of phosphoinositides, the targets of gasdermin-N, only in the cytoplasmic leaflet. To perform a similar assay in bacteria, we used protoplasts of Gram-positive *Bacillus megaterium* containing a single cardiolipin-containing membrane. The protoplasts were completely lysed by the GSDMD-(N+C) noncovalent complex, but not by full-length GSDMD or GSDMD-C (Extended Data Fig. 3f, g). PFO also caused no protoplast lysis, consistent with the absence of cholesterol in bacterial membranes. Similar results were obtained with the gasdermin-N domains of GSDMA and GSDMA3 (Extended Data Fig. 3g). Thus, membrane disruption by gasdermin-N correlates well with its lipid-binding properties.

Liposome leakage triggered by the gasdermin-N domain

We then tested the induction of liposome leakage by the gasdermin-N domain. The noncovalent complex of cleaved GSDMD or GSDMA3 caused around 50% leakage of PtdIns(4,5)P_2 liposomes (Extended Data Fig. 4a). The leakage reached 100% when PtdIns(4,5)P_2 was reconstituted into liposomes containing complicated phospholipid mixtures (Fig. 2a). Consistent with the binding data, GSDMA-N induced less liposome leakage (Fig. 2a and Extended Data Fig. 4a); liposome leakage reached about 50% with higher concentrations of GSDMA-N (Extended Data Fig. 4b). All three gasdermins caused nearly 100% leakage of the cardiolipin liposome (Fig. 2b). Full-length gasdermins and gasdermin-C did not lyse either type of liposome (Fig. 2a, b and Extended Data Fig. 4a). The gasdermins had no effect on cholesterol- or phosphatidylethanolamine-reconstituted liposomes (Fig. 2c and Extended Data Fig. 4c). As expected, PFO lysed cholesterol-containing liposomes but not those containing PtdIns(4,5)P_2 or cardiolipin (Fig. 2a–c and Extended Data Fig. 4a). These results are consistent with the finding that PFO but not gasdermin-N could lyse mammalian cells from the outside (Fig. 1d and Extended Data Fig. 3d). When liposomes encapsulating different-size fluorescent dextrans were assayed, the active forms of GSDMD, GSDMA3 and GSDMA could release dextrans with molecular masses of 3 or 10 kDa but not 40 kDa (Fig. 2d). This indicates that items with diameters of 10 nm or less can pass through the presumed pores formed by gasdermin-N.

Oligomerized gasdermin-N forms membrane pores

Full-length GSDMD, GSDMA3 and GSDMA were monomeric in solution (Extended Data Fig. 5a). Upon crosslinking of the GSDMD- or GSDMA3-(N+C) noncovalent complex or the GSDMA-N domain, GSDMD-N remained monomeric and GSDMA3/GSDMA-N showed a low degree of artificial oligomerization (Extended Data Fig. 5b). When crosslinking was performed after liposome incubation, all three gasdermin-N domains appeared as high-order oligomers (Extended Data Fig. 5b). As a control, PFO was converted from monomers into SDS-resistant oligomers after liposome incubation[19]. In LPS-stimulated pyroptotic iBMDMs, membrane-associated GSDMD-N, resulting from caspase-11 cleavage, also formed high-order oligomers, whereas full-length GSDMD and cytosolic GSDMD-N remained monomeric (Extended Data Fig. 5c). Similar results were obtained with the PPase-cleavable GSDMA in pyroptotic 293T cells (Extended Data Fig. 5c).

Negative-stain electron microscopy revealed multiple pores on nearly all cardiolipin liposomes that had been incubated with the GSDMD- or GSDMA3-(N+C) noncovalent complex, but not with full-length GSDMD or GSDMA3 (Fig. 3a). Similar (but fewer) membrane pores were formed on PtdIns(4,5)P_2-containing liposomes (Extended Data Fig. 5d); both intact and severely fragmented liposomes caused by merging of adjacent pores were observed. The pore-forming efficiency was markedly improved by reconstituting PtdIns(4,5)P_2 into liposomes containing the complicated phospholipid mixtures (Fig. 3a), consistent with the finding that these liposomes showed more severe leakage (Fig. 2a and Extended Data Fig. 4a). Furthermore,

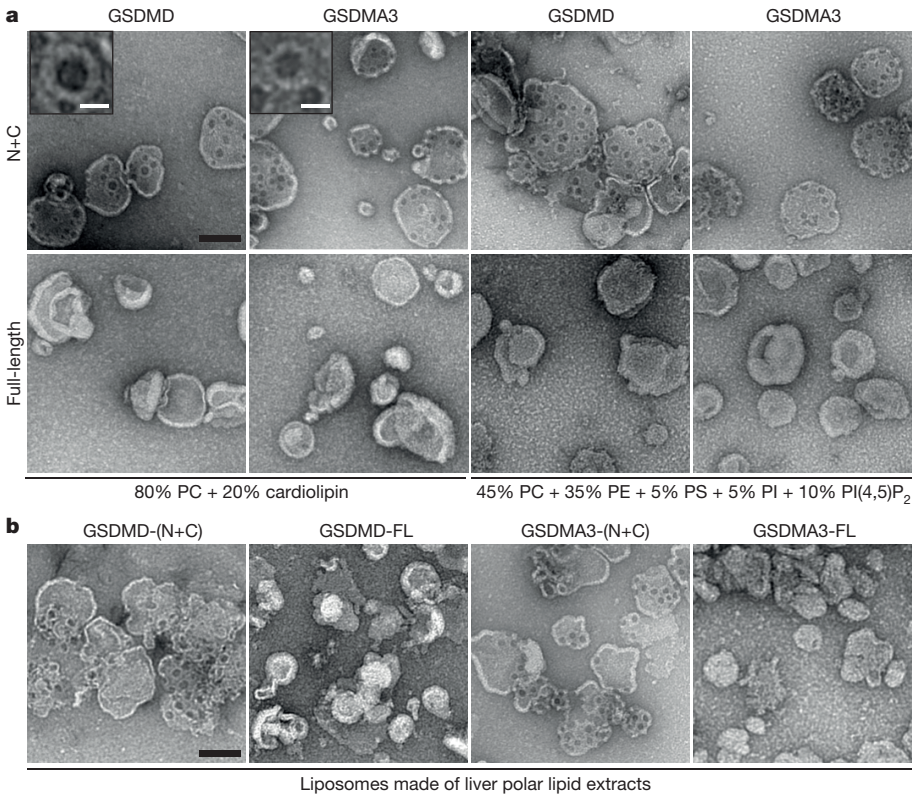

Figure 3 | Membrane pore-forming activity of the gasdermin-N domain. a, **b**, Liposomes with indicated lipid compositions (**a**) or prepared using bovine liver-derived polar lipid extracts (**b**) were treated with indicated gasdermin proteins. Shown are representative negative-stain electron microscopy micrographs of the liposomes (scale bar, 100 nm). Insets in **a**, expanded view of a representative pore (scale bar, 15 nm). All data shown are representative of three independent experiments.

the gasdermin-N domains of GSDMD, GSDMA3 and GSDMA could bind robustly to liposomes made of bovine liver or brain-derived lipid extracts (Extended Data Fig. 2f) and accordingly generated similar pores on the liposomes (Fig. 3b).

Of the GSDMD-induced pores, 60% had inner diameters of 10–16 nm whereas all GSDMA3-induced pores had inner diameters of 10–14 nm (Extended Data Fig. 6a, b). Decreasing the gasdermin concentration by 10-fold affected the number but not the size distribution of the pores (Extended Data Fig. 6a, b). The pore size is consistent with the assessment from the dextran leakage data (Fig. 2d). The wider pore-size range produced by GSDMD, compared with GSDMA3, probably resulted from the less optimal properties of recombinant GSDMD. Previously, the inner diameter of membrane pores in caspase-1-mediated pyroptosis was estimated to be 1.1–2.4 nm, on the basis of the observation that PEG2000 but not PEG200, at an equal molar concentration, can block pyroptosis[20]. We confirmed this finding but further found that increasing the mass concentration of PEG200 to the same as PEG2000 (to ensure equal osmotic potential) could generate the same protective effect (Extended Data Fig. 6c). Considering that gasdermin-N formed similar pores on liposomes made of natural lipid extracts, pores with inner diameters of 10–14 nm are likely to predominate *in vivo*. This pore size can allow the passage of mature IL-1β (also IL-18) and caspase-1, which have diameters of 4.5 and 7.5 nm, respectively. GSDMD-N and GSDMA3-N also formed pores on lipid monolayers; GSDMA3-N pores had a uniform inner diameter of about 14 nm (Extended Data Fig. 6d). Following 2D classification, one class of GSDMA3 pores showed the best protein contrast, and subsequent rotational auto-correlation analysis revealed 16-fold symmetry (Extended Data Fig. 6e). Given the single-layer property of all known pore-forming complexes, these data suggest that the gasdermin-N domain forms a 16-mer pore complex.

Crystal structure of GSDMA3

We determined the 1.90 Å crystal structure of GSDMA3 (Extended Data Table 1 and Extended Data Fig. 7a).The structure is separated into two domains—the presumed gasdermin-N and gasdermin-C domains (Fig. 4a). Gasdermin-N mainly contains an extended twisted β-sheet formed by nine tandem strands (β3–β11) (Fig. 4a and Extended Data Fig. 7b). The N-terminal α1 helix and following β1–β2 hairpin lie in the concave of the β-sheet. Helices α2 and α3 flank the β-sheet at one end. Helix α4 protrudes away from the other end of the β-sheet through two loops to contact the helical gasdermin-C domain. The C domain adopts a compact globular fold covered by a short three-stranded β-sheet (β12–β14). The long loop (residues 234–263) linking the GSDMA3-N and -C domains stretches away from the main body of the structure. A structural homology search[21] revealed no meaningful information about gasdermin-C; the structure of gasdermin-N also showed no convincing similarity to any known proteins, suggesting that it represents a new type of pore-forming protein.

Functional analyses of GSDMA3 autoinhibition

In the structure, the α1 helix and β1–β2 hairpin in GSDMA3-N provide the primary surface for binding to the GSDMA3-C domain (Fig. 4b). F48 and W49 from the hairpin loop are inserted deeply into a groove in GSDMA3-C and encircled by L270, Y344, A348 and A443, forming a hydrophobic core (Fig. 4c). In addition, R43, K44 and T46 from the hairpin have four hydrogen bonds with E273, E277 and D340; α1 also supplies D6 and R13 for hydrogen-bonding with H436 and D433. At the second inter-domain interface, α4 presents its hydrophobic face (L181, L184 and L186) to a non-polar surface formed by α9 and α11 in GSDMA3-C (Fig. 4c). Nine *Gsdma3* mutations that can cause alopecia and hyperkeratosis in mice have been identified[14–16]. Among them, 259RDW (insertion after residue 259 with three mistranslated residues RDW) and 366stop (a premature stop at residue 366) encode truncated GSDMA3 devoid of inter-domain contacts; Y344C, Y344H and A348T are mutations in residues that directly contact GSDMA3-N; T278P and L343P are near the direct-contacting residues; and 412EA (duplication of E411A412) disrupts the α4-binding surface. Consistently, T278P, L343P, Y344C, A348T and 412EA all weaken inter-domain interactions, resulting in constitutive activation of GSDMA3 (ref. 10). Similarly, GSDMA3 L270D, Y344D and A348D exhibited spontaneous pyroptosis-inducing activity (Fig. 4d).

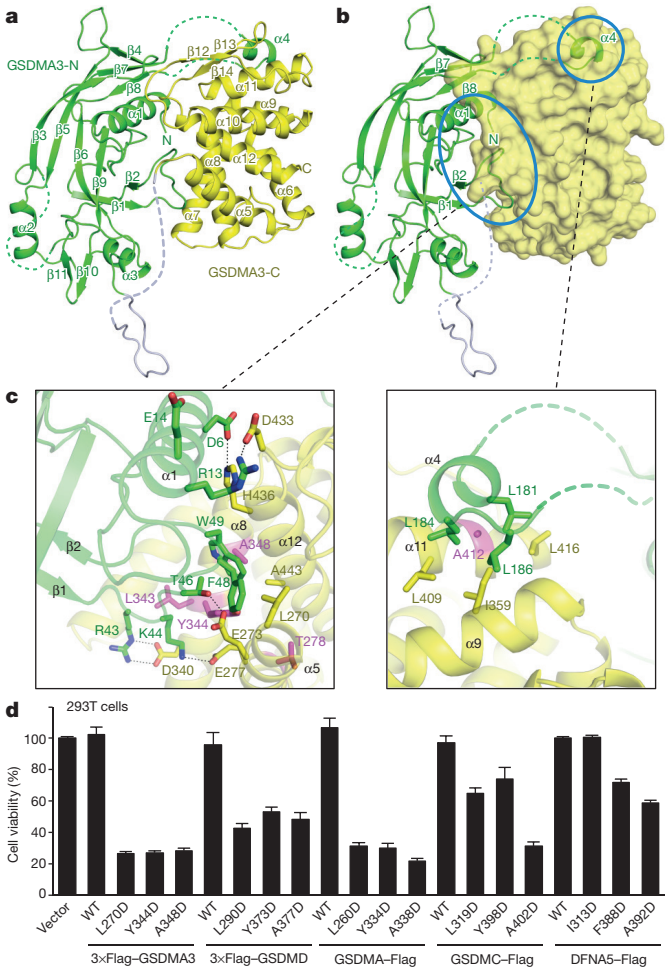

Figure 4 | Crystal structure of GSDMA3 and structural autoinhibition of the gasdermin family. a, **b**, Overall structure of GSDMA3 and the inter-domain interfaces. The gasdermin-N (GSDMA3-N) and gasdermin-C (GSDMA3-C) domains are coloured green and yellow, respectively. Structures of GSDMA3-N (**a**, **b**) and GSDMA3-C (**a**) are shown as cartoon models, and that of GSDMA3-C (**b**) is in a transparent surface scheme. Secondary structure elements are labelled in **a**. The primary and second inter-domain interfaces are highlighted by large and small blue ellipses, respectively (**b**). Disordered loops are indicated by dashed lines. **c**, Close-up view of the autoinhibitory interactions. Left and right, primary and secondary inter-domain interfaces, respectively. Residues involved in the autoinhibitory interactions are labelled and shown as sticks. Point mutations in GSDMA3 that cause alopecia in mice are coloured pink. Dotted lines, hydrogen bonds. **d**, Mutation analyses of the autoinhibitory contacts. Full-length GSDMA3, GSDMD, GSDMA, GSDMC or DFNA5 (wild type (WT) or containing indicated point mutations in their gasdermin-C domains) was transfected into 293T cells. ATP-based cell viability is expressed as mean ± s.d. from three technical replicates; data are representative of three independent experiments.

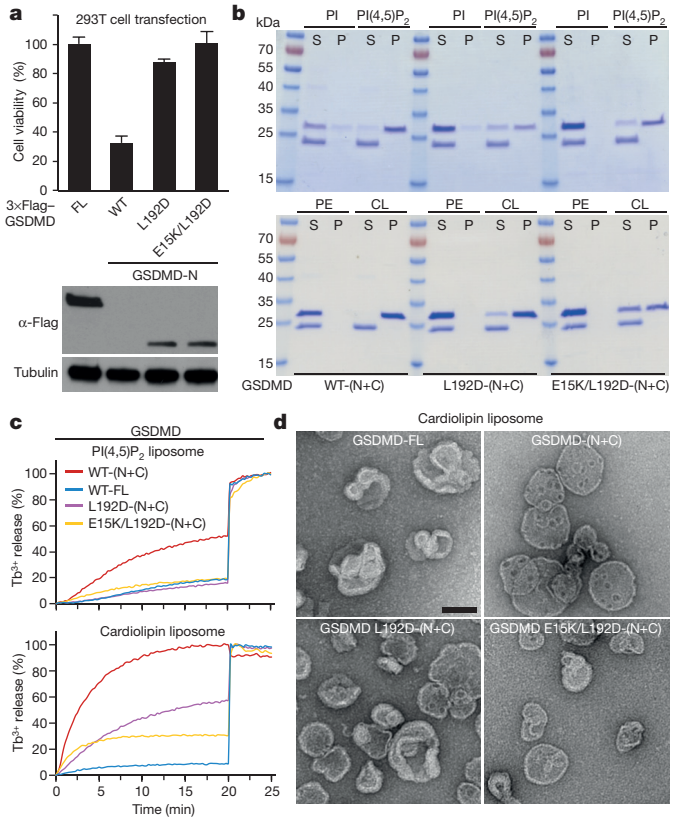

Figure 5 | Residues in the autoinhibited region in gasdermin-N are important for pyroptosis, membrane disruption and pore formation. a, Effects of L192D/E15K mutations in GSDMD-N on pyroptosis-inducing activity. Full-length GSDMD or GSDMD(1–275) (wild type or with indicated mutations) was transfected into 293T cells. ATP-based cell viability is expressed as mean ± s.d. from three technical replicates. The immunoblot shows expression of transfected GSDMD. **b**, **c**, Effects of L192D/E15K mutations on GSDMD-N lipid-binding and liposome-leakage-inducing activities. Purified GSDMD proteins were incubated with liposomes containing 80% phosphatidylcholine and 20% phosphatidylinositol, PtdIns(4,5)P_2, phosphatidylethanolamine or cardiolipin. After ultracentrifugation, the liposome-free supernatant (S) and the liposome pellet (P) were analysed by SDS–PAGE (**b**). Liposome leakage was monitored by measuring DPA chelating-induced fluorescence of released Tb^{3+} relative to that of Triton X-100 treatment (**c**). **d**, Effects of L192D/E15K mutations on pore formation by GSDMD-N. Shown are representative negative-stain electron microscopy micrographs of pores formed by indicated GSDMD proteins on cardiolipin liposomes (scale bar, 100 nm). All data shown are representative of three independent experiments.

Conserved autoinhibition in the gasdermin family

GSDMD shares about 70% homology with GSDMA3. Homology-based modelling produced a highly analogous GSDMD structure (Extended Data Fig. 7c). The structure contains a hydrophobic core resembling that in GSDMA3, in which F49/W50 play equivalent roles to F48/W49 in GSDMA3. The modelled structure bears a similar second inter-domain contact; an α4-equivalent helix has extensive hydrophobic interactions with GSDMD-C despite the residues involved being different. The residues in gasdermin-C that make the hydrophobic core are highly conserved in the gasdermin family (Extended Data Fig. 8), including above analysed L270, Y344 and A348 in GSDMA3. When equivalent residues in GSDMD (L290, Y373 and A377), GSDMA (L260, Y334 and A338), GSDMC (L319, Y398 and A402) and DFNA5 (I313, F388 and A392) were individually mutated into aspartates, 20–80% pyroptosis occurred in 293T cells expressing the mutant proteins (except for DFNA5 I313D) (Fig. 4d). Thus, structural autoinhibition is conserved in most gasdermins.

Structure–based analyses of gasdermin–N function

L184 in GSDMA3-N (L192 in GSDMD-N) on the α4 helix is contacted by the inhibitory gasdermin-C domain (Fig. 4c and Extended Data Fig. 7c). E14 in GSDMA3-N (E15 in GSDMD-N) on helix α1 is within the primary inter-domain interface (Fig. 4c). Mutations of gasdermin-C residues that contact L184 or structural regions around E14 caused constitutive activation of GSDMA3 and GSDMD[10] (Fig. 4d). As these mutations will disrupt the autoinhibition and expose L184/E14, we reasoned that L184/E14 or their adjacent residues might be important for pyroptosis. Supporting this prediction, GSDMD-N(L192D) and GSMDA3-N(L184D) induced markedly decreased pyroptosis in 293T cells (Fig. 5a and Extended Data Fig. 9a). The mutants showed evident defects in binding the liposome and causing the liposome

leakage (Fig. 5b, c and Extended Data Fig. 9b, c). Combining the L/D mutation with the also partially inactive E15K mutation on GSDMD (E14K on GSDMA3) led to further decreased liposome binding and leakage-inducing activities. Double mutants of the GSDMD- and GSDMA3-(N+C) complexes formed fewer pores than the L/D single mutant (Fig. 5d and Extended Data Fig. 9d). GSDMD-N(L192D/E15K) and GSDMA3-N(L184D/E14K) were largely deficient in pyroptosis induction (Fig. 5a and Extended Data Fig. 9a). The two residues probably participate in oligomerization and membrane insertion during pore formation. These data reinforce the idea that the liposome-leakage and pore-forming activities of gasdermin-N are responsible for cell pyroptosis.

Discussion

We show that multiple gasdermin-N domains can induce pyroptosis owing to their pore-forming activity. Most gasdermin pores have inner diameters of 10–14 nm. The structure of GSDMA3 uncovers an autoinhibitory mechanism that is conserved in the gasdermin family. Other members of the gasdermin family may also act on endomembranes and alter other cellular physiologies. Indeed, DFNB59 and DFNA5 have been suggested to localize on the peroxisomes and mitochondria, respectively[22,23].

The gasdermin-N domain represents a new type of pore-forming protein (PFP). PFPs are diverse in sequence and present in many domains of life[24]. Most PFPs lyse cell membranes from the outside. By contrast, gasdermins and the MLKL protein (which is involved in necroptosis) kill cells from the cytosol. MLKL can induce liposome leakage, but there is no reported evidence that it can form pores[25–28]. PFPs can be divided into α-helical and β-barrel classes on the basis of the structures of their membrane-spanning regions[29]. The structure of gasdermin-N differs completely from those of α-class PFPs. A Dali search of the GSDMA3-N structure produced hits all belonging to the membrane-attack complex/perforin/cholesterol-dependent cytolysin (MACPF/CDC) family of β-class PFPs[30], but the score was not confident and no meaningful structural similarity could be identified (Extended Data Fig. 7d). Gasdermin-N is likely to use either a β-barrel-like or a distinct mechanism for pore formation, which will involve drastic conformational changes for insertion into the membrane. Our results pave the way for future studies to elucidate the structural mechanism of pore formation by gasdermins.

Online Content Methods, along with any additional Extended Data display items and Source Data, are available in the online version of the paper; references unique to these sections appear only in the online paper.

Received 6 March 2015; accepted 18 May 2016.
Published online 8 June; corrected online 10 June 2016 (see full-text HTML version for details).

1. Jorgensen, I. & Miao, E. A. Pyroptotic cell death defends against intracellular pathogens. *Immunol. Rev.* **265,** 130–142 (2015).
2. Cookson, B. T. & Brennan, M. A. Pro-inflammatory programmed cell death. *Trends Microbiol.* **9,** 113–114 (2001).
3. Shi, J. *et al.* Inflammatory caspases are innate immune receptors for intracellular LPS. *Nature* **514,** 187–192 (2014).
4. Kayagaki, N. *et al.* Non-canonical inflammasome activation targets caspase-11. *Nature* **479,** 117–121 (2011).
5. Lamkanfi, M. & Dixit, V. M. Mechanisms and functions of inflammasomes. *Cell* **157,** 1013–1022 (2014).
6. Zhao, Y. & Shao, F. Diverse mechanisms for inflammasome sensing of cytosolic bacteria and bacterial virulence. *Curr. Opin. Microbiol.* **29,** 37–42 (2016).
7. Hagar, J. A., Powell, D. A., Aachoui, Y., Ernst, R. K. & Miao, E. A. Cytoplasmic LPS activates caspase-11: implications in TLR4-independent endotoxic shock. *Science* **341,** 1250–1253 (2013).
8. Kayagaki, N. *et al.* Noncanonical inflammasome activation by intracellular LPS independent of TLR4. *Science* **341,** 1246–1249 (2013).
9. Yang, J., Zhao, Y. & Shao, F. Non-canonical activation of inflammatory caspases by cytosolic LPS in innate immunity. *Curr. Opin. Immunol.* **32,** 78–83 (2015).
10. Shi, J. *et al.* Cleavage of GSDMD by inflammatory caspases determines pyroptotic cell death. *Nature* **526,** 660–665 (2015).
11. Kayagaki, N. *et al.* Caspase-11 cleaves gasdermin D for non-canonical inflammasome signalling. *Nature* **526,** 666–671 (2015).
12. Saeki, N. & Sasaki, H. in *Endothelium and Epithelium: Composition, Functions, and Pathology* (eds Carrasco, J. & Matheus, M.) Ch. IX, 193–211 (Nova Science Publishers, 2011).
13. Tanaka, S., Mizushina, Y., Kato, Y., Tamura, M. & Shiroishi, T. Functional conservation of *Gsdma* cluster genes specifically duplicated in the mouse genome. *G3 (Bethesda)* **3,** 1843–1850 (2013).
14. Sato, H. *et al.* A new mutation *Rim3* resembling *Re*^{den} is mapped close to retinoic acid receptor alpha (*Rara*) gene on mouse chromosome 11. *Mamm. Genome* **9,** 20–25 (1998).
15. Porter, R. M. *et al.* Defolliculated (dfl): a dominant mouse mutation leading to poor sebaceous gland differentiation and total elimination of pelage follicles. *J. Invest. Dermatol.* **119,** 32–37 (2002).
16. Runkel, F. *et al.* The dominant alopecia phenotypes Bareskin, Rex-denuded, and Reduced Coat 2 are caused by mutations in *gasdermin 3*. *Genomics* **84,** 824–835 (2004).
17. Van Laer, L. *et al.* Nonsyndromic hearing impairment is associated with a mutation in *DFNA5*. *Nat. Genet.* **20,** 194–197 (1998).
18. Delmaghani, S. *et al.* Mutations in the gene encoding pejvakin, a newly identified protein of the afferent auditory pathway, cause DFNB59 auditory neuropathy. *Nat. Genet.* **38,** 770–778 (2006).
19. Shepard, L. A., Shatursky, O., Johnson, A. E. & Tweten, R. K. The mechanism of pore assembly for a cholesterol-dependent cytolysin: formation of a large prepore complex precedes the insertion of the transmembrane beta-hairpins. *Biochemistry* **39,** 10284–10293 (2000).
20. Fink, S. L., Bergsbaken, T. & Cookson, B. T. Anthrax lethal toxin and *Salmonella* elicit the common cell death pathway of caspase-1-dependent pyroptosis via distinct mechanisms. *Proc. Natl Acad. Sci. USA* **105,** 4312–4317 (2008).
21. Holm, L. & Rosenström, P. Dali server: conservation mapping in 3D. *Nucleic Acids Res.* **38,** W545–W549 (2010).
22. Delmaghani, S. *et al.* Hypervulnerability to sound exposure through impaired adaptive proliferation of peroxisomes. *Cell* **163,** 894–906 (2015).
23. Van Rossom, S., Op de Beeck, K., Hristovska, V., Winderickx, J. & Van Camp, G. The deafness gene *DFNA5* induces programmed cell death through mitochondria and MAPK-related pathways. *Front. Cell. Neurosci.* **9,** 231 (2015).
24. Bischofberger, M., Iacovache, I. & van der Goot, F. G. Pathogenic pore-forming proteins: function and host response. *Cell Host Microbe* **12,** 266–275 (2012).
25. Hildebrand, J. M. *et al.* Activation of the pseudokinase MLKL unleashes the four-helix bundle domain to induce membrane localization and necroptotic cell death. *Proc. Natl Acad. Sci. USA* **111,** 15072–15077 (2014).
26. Dondelinger, Y. *et al.* MLKL compromises plasma membrane integrity by binding to phosphatidylinositol phosphates. *Cell Reports* **7,** 971–981 (2014).
27. Wang, H. *et al.* Mixed lineage kinase domain-like protein MLKL causes necrotic membrane disruption upon phosphorylation by RIP3. *Mol. Cell* **54,** 133–146 (2014).
28. Cai, Z. *et al.* Plasma membrane translocation of trimerized MLKL protein is required for TNF-induced necroptosis. *Nat. Cell Biol.* **16,** 55–65 (2014).
29. Iacovache, I., Bischofberger, M. & van der Goot, F. G. Structure and assembly of pore-forming proteins. *Curr. Opin. Struct. Biol.* **20,** 241–246 (2010).
30. Reboul, C. F., Whisstock, J. C. & Dunstone, M. A. Giant MACPF/CDC pore forming toxins: A class of their own. *Biochim. Biophys. Acta* **1858,** 475–486 (2016).

Supplementary Information is available in the online version of the paper.

Acknowledgements We thank W. Wei for reagents, H. Wang for suggestions on electron microscopy data analysis, and the staff of beamlines BL18U1 and BL19U1 at National Center for Protein Sciences, Shanghai, and Shanghai Synchrotron Radiation Facility for X-ray data collection. This work was supported by grants from the Strategic Priority Research Program of the Chinese Academy of Sciences (XDB08020202), the China National Science Foundation Program for Distinguished Young Scholars (31225002) and Program for International Collaborations (31461143006), and the National Basic Research Program of China 973 Program (2012CB518700 and 2014CB849602) to F.S. The research was also supported in part by an International Early Career Scientist grant from the Howard Hughes Medical Institute and the Beijing Scholar Program to F.S.

Author Contributions J.D., D.-C.W. and F.S. conceived the study; J.D., together with K.W., designed and performed the majority of the experiments; Y.S. helped with protein purification; W.L. performed the pyroptosis assay; Q.S. assisted J.D. in electron microscopy studies; J.S. provided critical reagents and suggestions; H.S. performed structural modelling; and J.D. and F.S. analysed the data and wrote the manuscript. All authors discussed the results and commented on the manuscript.

Author Information The atomic coordinates and structure factors of GSDMA3 have been deposited in the Protein Data Bank under the accession code 5B5R. Reprints and permissions information is available at www.nature.com/reprints. The authors declare no competing financial interests. Readers are welcome to comment on the online version of the paper. Correspondence and requests for materials should be addressed to D.-C.W. (dcwang@sun5.ibp.ac.cn) or F.S. (shaofeng@nibs.ac.cn).

Reviewer Information *Nature* thanks F. Sigworth and the other anonymous reviewer(s) for their contribution to the peer review of this work.

METHODS

The experiments were not randomized. The investigators were not blinded to allocation during experiments and outcome assessment.

Plasmids, antibodies and reagents. Complementary DNA (cDNA) for human *GSDMA*, *GSDMB*, *GSDMC*, *GSDMD* and mouse *Gsdma3* were previously described[10]; cDNA for human *DFNA5* was obtained from Life Technologies Ultimate ORF collection (IOH41276). The cDNAs were inserted into a modified pCS2 vector with an N-terminal 3 × Flag tag or the pcDNA3 vector with a C-terminal Flag tag for transient expression in 293T cells and the pWPIlentiviral vector with an N-terminal 2 × Flag-HA tag for stable expression in iBMDM cells. For Tet-On expression, the cDNAs were inserted into a modified pLenti–NIrD vector (a gift from W. Wei) harbouring the blasticidin-resistance gene and fused with a C-terminal eGFP tag. For growth inhibition in *E. coli*, the cDNAs were cloned into the pET21a vector. For recombinant expression in *E. coli*, the cDNAs were cloned into a modified pET vector with an N-terminal 6 × His-SUMO tag or pGEX-6P-2 with an N-terminal GST tag. DNA for PFO was amplified from genomic DNA of *C. perfringens*. For recombinant expression of PFO in *E. coli*, the DNA was cloned into a pET28a vector with an N-terminal 6 × His tag. Truncation mutants of gasdermins were constructed by the standard PCR cloning strategy and inserted into the corresponding vectors with indicated tags. Point mutations were generated by the QuickChange Site-Directed Mutagenesis Kit (Stratagene). All plasmids were verified by DNA sequencing.

Antibodies used in this study include anti-Flag M2 (F4049), anti-actin (A2066) and anti-tubulin (T5168) (Sigma-Aldrich); anti-TOM20 (sc-11415) and anti-Lamp2 (sc-18822) (Santa Cruz Biotechnology); anti-Cox4 (11967, Cell Signaling Technology); anti-LAMP1 (553792) and anti-sytaxin 6 (610635) (BD Pharmingen); and anti-Na and K-ATPase α1 (2047-1, Epitomics). Rabbit antiserum for the GSDMD-C domain was generated in our in-house facility. Natural and synthetic lipid products used for liposome preparation were purchased from Avanti Polar Lipids Inc. Lipid strips used in the protein-lipid overlay assay were obtained from Echelon Biosciences Inc. Fluorescein-labelled dextran was from Life Technologies. LPS (L4524), terbium chloride ($TbCl_3$) and DPA were purchased from Sigma-Aldrich. Cell culture products were from Life Technologies and all other chemicals used were from Sigma-Aldrich unless noted.

Cell culture and transfection. HeLa and 293T cells were obtained from the American Type Culture Collection (ATCC). C57BL/6 mouse-derived wild-type and *Gsdmd*$^{-/-}$ iBMDM cells were as described[10].The cells are frequently checked by virtue of their morphological features and functionalities but have not been subjected to authentication by short tandem repeat (STR) profiling. All cell lines have been tested to be mycoplasma-negative by the commonly used PCR method. Cells were grown in DMEM supplemented with 10% (v/v) fetal bovine serum (FBS) and 2 mM L-glutamine at 37 °C in a 5% CO_2 incubator. Transient transfection in HeLa and 293T cells was performed using the JetPRIME (Polyplus Transfection) or Vigofect (Vigorous) reagents following the manufacturers' instructions. iBMDM or HeLa stable cell lines were generated by lentiviral infection as previously described[10]. Stable expression cells were sorted by flow cytometry (BD Biosciences FACSAria II) or selected by 60 μg ml^{-1} blasticidin (Invitrogen).

Microscopy imaging. To examine morphology of pyroptotic cells, cells were treated as indicated in 6-well plates (NuncProducts, Thermo Fisher Scientific Inc.). Static brightfield images of pyroptotic cells were captured using an Olympus IX71 microscope. To examine the subcellular localization of the gasdermin N-domain during pyroptosis, HeLa cells harbouring the desired Tet-On expression plasmid were treated with 2 μg ml^{-1} doxycycline in glass-bottom culture dishes (MatTek Corporation). After 3 h, live images of pyroptotic cells were recorded with a PerkinElmer UltraVIEW spinning disk confocal microscope and processed in the Volocity program. All image data shown are representative of at least three randomly selected fields.

Cell viability and osmotic protection. For viability assay, relevant cells were treated as indicated and the viability was determined by the CellTiter-Glo Luminescent Cell Viability Assay (Promega). To examine effects of osmotic protection, iBMDM cells harbouring a sensitive *Nlrp1b* allele were treated with 1.2% or 12% (w/v) osmoprotectants (PEG200, PEG1500 or PEG2000) or 40 μM zVAD for 1 h. Pyroptosis was induced by LFn-BsaK[31] or anthrax lethal toxin stimulation[32], which activate the NAIP2/NLRC4 inflammasome or NLRP1B inflammasome, respectively. Cell death was measured by the LDH release assay using the CytoTox 96 Non-Radioactive Cytotoxicity Assay kit (Promega).

Cell fractionation by differential centrifugations. Cells were collected by centrifugation at 1,000*g* for 10 min. The washed cell pellets were resuspended in 5 volumes of buffer A (20 mM HEPES, pH 7.5, 40 mMKCl, 1.5 mM $MgCl_2$, 1 mM EDTA and 250 mM sucrose) and incubated on ice for 30 min. The cells were homogenized by passing through a 22G needle 24 times. After centrifugation at 1,000*g* for 10 min, the supernatant was collected and re-centrifuged at 7,000*g* for 10 min. The supernatant and pellet were designated as the S7 and P7 fraction, respectively. The S7 fraction was centrifuged again at 20,000*g* for 20 min to obtain the S20 and P20 fractions. The S20 fraction was subjected to final centrifugation at 100,000*g* for 1 h and the supernatant was collected as the S100 fraction. The pellet was dissolved in buffer A as the P100 fraction. All centrifugations were performed at 4 °C. The fractions were solubilized in SDS loading buffer and analysed by immunoblotting as indicated.

Purification of recombinant proteins. To obtain full-length GSDMD, GSDMA and GSDMA3 proteins, *E. coli* BL21 (DE3) cells harbouring the gasdermin plasmid (pET28a-6 × His-SUMO vector) were grown in LB medium supplemented with 30 μg ml^{-1} kanamycin. Protein expression was induced overnight at 20 °C with 0.4 mM IPTG after OD_{600} reached 0.8. Cells were lysed in the buffer containing 20 mM Tris-HCl (pH 8.0), 300 mM NaCl, 20 mM imidazole and 10 mM 2-mercaptoethanol. The fusion protein was affinity-purified by Ni-Sepharose beads (GE Healthcare Life Sciences). The SUMO tag was removed by overnight digestion with homemade ULP1 protease at 4 °C. The untagged protein was further purified by HiTrap Q anion exchange and Superdex G75 gel filtration chromatography (GE Healthcare Life Sciences). Selenomethionine-substituted (SeMet) GSDMA3 was expressed in the methionine auxotrophic *E. coli* strain B834 (DE3) and purified in the same way as the native protein.

The engineered gasdermin proteins (GSDMD, GSDMA and GSDMA3) containing the PreScission protease (PPase) recognition site were expressed and purified by following the same procedure as that for native gasdermin proteins. Inter-domain cleavage was performed by overnight digestion with homemade PPase at 4 °C. The proteins were further purified by Superdex G75 gel-filtration chromatography to obtain high-quality noncovalent complex of the cleaved gasdermin. To obtain the GSDMA-N domain alone, the noncovalent complex of GSDMA was further subjected to HiTrap Q anion exchange chromatography, followed by another round of Superdex G75 gel filtration chromatography. To obtain the gasdermin-C domain of GSDMA3 and GSDMA, the flow-through fractions of PPase-cleaved GSDMA3 and GSDMA proteins from Ni-Sepharose beads were subjected to HiTrap Q anion exchange and Superdex G75 gel filtration chromatography. To obtain GSDMD-C protein, *E. coli* BL21 (DE3) cells were transformed with pGEX-6P-2-GSDMD (residues 276–484). The GST-tagged protein was purified by affinity chromatography using glutathione-Sepharose beads (GE Healthcare Life Sciences) and the tag was removed by overnight digestion with PPase at 4 °C. The proteins were further purified by Superdex G75 gel filtration chromatography. Recombinant PFO was expressed and purified by following the same procedure as that for the gasdermin protein. All the purified proteins were concentrated and stored in the buffer containing 20 mM HEPES (pH 7.5), 150 mM NaCl and 5 mM dithiothreitol.

Bacterial growth inhibition and protoplast lysis. To assay the cytotoxicity of the gasdermin-N domain in *E. coli*, equal amounts of *E. coli* BL21 (DE3) cells were transformed with 0.1 μg of indicated plasmid. The transformed cells were serially diluted and plated onto LB agar containing the appropriate antibiotics in the presence or absence of IPTG. The colony-forming unit (CFU) was determined by counting the number of viable bacteria per transformation after overnight culture at 37 °C.

To prepare the protoplast, *B. megaterium* cells were grown in AB3 medium (DIFCO) at 37 °C until the OD_{600} reached 2.0. The centrifuged bacterial pellets, resuspended in the buffer containing 20 mM sodium malate (pH 6.5), 20 mM $MgCl_2$ and 500 mM sucrose, were incubated with 2 mg ml^{-1} lysozyme at 37 °C until protoplast formation was complete (judged under phase-contrast microscopy).The protoplasts were diluted to an OD_{600} of 1.0. To assay protoplast lysis, aliquots of the protoplasts (1.9 ml) were incubated with 100 μl of indicated gasdermin proteins (final concentration of 0.6 μM) at 37 °C for 30 min. To achieve complete lysis of the protoplast, 100 μl of 2% (v/v) Triton X-100 was added. The OD_{600} of each protoplast aliquot before and after incubation with the gasdermin protein was measured and defined as $A_0$and A_n, respectively, and that after Triton X-100 treatment was treated as A_{100}. The percentage of protoplast lysis is defined as: lysis (%) = $(A_0 - A_n) \times 100/(A_0 - A_{100})$. For the time-course plot of protoplast lysis, the OD_{600} of each protoplast aliquot was continuously recorded for 15 min at 1-min intervals before Triton X-100 was added.

Liposome preparation. Phospholipids and phosphoinositides were dissolved in chloroform and chloroform-methanol mixture (20:9, v-v), respectively. Lipids with indicated compositions (0.5 μmol) were mixed in a glass vial. The solvent was evaporated under a stream of nitrogen, and the dry lipid film was then hydrated at room temperature with constant mixing in 500 μl buffer 1 (20 mM HEPES (pH 7.5) and 150 mM NaCl). Liposomes were generated by extrusion of the hydrated lipids through a 100-nm polycarbonate filter (Whatman) 35 times using the Mini-Extruder device (Avanti Polar Lipids Inc.). For Tb^{3+}-encapsulated liposomes, the lipid film was hydrated with 500 μl buffer 2 (20 mM HEPES (pH 7.5), 100 mM NaCl, 50 mM sodium citrate and 15 mM $TbCl_3$). After the extrusion

process, Tb^{3+} ions outside the liposome were removed by repeated washing with buffer 2 on a centrifugal filter device (Amicon Ultra-4, 100K MWCO, Millipore). The liposomes were subjected to buffer change into buffer 1 for use. To prepare dextran-encapsulated liposomes, the lipid film was hydrated in buffer 1 supplemented with 2 mg ml^{-1} dextrans. The liposomes were repeatedly washed to remove external dextran and then resuspended in 500 μl buffer 1. All the liposomes were stored at 4 °C and used within 48 h.

Liposome-binding and leakage assays. The indicated gasdermin proteins (5 μM) were incubated with the indicated liposome (500 μM lipids) at room temperature for 30 min in a total volume of 80 μl. Samples were centrifuged in a Beckman Optima MAX-XP ultracentrifuge at 4 °C for 20 min at 100,000*g*. The supernatant (S) was collected to examine proteins not bound to the liposome. The pellets (P) were washed twice with 100 μl buffer 1 by re-centrifugation and brought up to the same volume as the supernatant. The S and P fractions were analysed by SDS–PAGE followed by Coomassie blue staining.

For liposome leakage assay, aliquots of Tb^{3+}-encapsulated liposomes were diluted to 300 μM lipid concentration in 90 μl of buffer 1 supplemented with 15 μM DPA. The excitation and emission wavelengths of 270 nm and 490 nm, respectively, were used to examine the Tb^{3+}/DPA chelates[33]. The emission fluorescence before adding the gasdermin protein was treated as F_{t0}. 10 μl of protein was then added to a final concentration of 0.6 μM, and the emission fluorescence was continuously recorded as F_t at 15-s intervals. After 20 min, 10 μl of 1% Triton X-100 was added to achieve complete release of Tb^{3+}, and mean values of the top three fluorescence reads were defined as F_{t100}. The percentage of liposome leakage at each time point is defined as: leakage (t) (%) $= (F_t - F_{t0}) \times 100/(F_{t100} - F_{t0})$. For dextran leakage assay, aliquots of dextran-encapsulated liposomes (300 μM of lipids) were incubated with 0.6 μM indicated proteins at room temperature for 30 min in a total volume of 100 μl. After centrifugation, the released dextran in the supernatants was collected and the emission fluorescence (521 nm) after excitation at 494 nm was measured as F_n. The emission fluorescence of supernatants of untreated liposomes was measured as F_0, and that of the liposomes solubilized with 0.1% Triton X-100 was defined as F_{100}. The percentage of dextran leakage is defined as: leakage (%) $= (F_n - F_0) \times 100/(F_{100} - F_0)$.

Crosslinking assays of gasdermin-N oligomerization. To assay gasdermin-N domain oligomerization *in vitro*, indicated PPase-cleaved engineered gasdermin proteins, before or after incubation with the liposome, were treated with 5 mM glutaraldehyde for 30 min at room temperature. The liposome pellets were solubilized in SDS loading buffer. Samples with or without crosslinking were analysed by SDS-agarose gel electrophoresis as previously described[19]. To assay the oligomerization during pyroptosis, relevant cells, before or after pyroptosis induction, were harvested in PBS. The cell pellets were homogenized by passing through a 22G needle 24 times. Cell lysates were centrifuged at 100,000*g* for 1 h to obtain the supernatant and the pellet fractions. The pellet was homogenized by gentle sonication. Both fractions were treated with 2 mM glutaraldehyde at room temperature for 15 min. Samples with or without crosslinking were analysed by both SDS-agarose and SDS–PAGE gel electrophoresis followed by immunoblotting.

Electron microscopy and image processing. Gasdermin proteins (5 μM) were incubated with indicated liposomes (500 μM of lipids) at room temperature for 30 min. Aliquots of the mixture (5 μl) were transferred to carbon support films on electron microscopy grids and negatively stained with 2% uranyl acetate. Samples were imaged on a Tecnai T12 microscope (FEI) at 120 kV. Images were taken on a Gatan 4k × 4k CCD camera with a nominal magnification of 30,000×, giving a final pixel size of 3.71 Å. To prepare pores on lipid monolayers, solutions of noncovalent complexes of cleaved GSDMD (500 nM) and GSDMA3 (100 nM) were pipetted into Teflon wells and coated with a droplet of 1 mM lipid mixture containing 80% phosphatidylcholine and 20% cardiolipin in chloroform. Negative-stain electron microscopy of the GSDMA3 pores was performed and images were captured as above described. Complete and undistorted pore particles were manually selected from the micrographs using EMAN2 (ref. 34). A total of 7,056 particle images were collected and normalized. After determining the defocus, the particles were phase-flipped for contrast transfer function correction using EMAN2 (ref. 34). Two-dimensional reference-free classification was then performed in Relion1.3 (ref. 35). More than 80% of class averages were pores of a uniform size around 30 nm in diameter. The averaged view with the best particle contrast of a class comprising 242 particles was selected and its rotational auto-correlations were calculated in SPIDER[36] to determine the symmetry.

Structure determination. The crystallization experiments were performed using the sitting-drop vapour diffusion method at 20 °C with 2-μl drops containing 1 μl protein solution and 1 μl reservoir solution equilibrated over 100 μl reservoir solution. Initial crystallization hits of GSDMA3 were found from the Index Kit (Hampton Research) screen. Qualified crystals of SeMet-labelled GSDMA3 were obtained in the reservoir buffer containing 100 mMBis-Tris (pH 6.5), 19% polyethylene glycol 3550, and 10 mM TCEP within 2 weeks. For data collection, the crystals were soaked in a cryoprotectant solution containing the reservoir buffer supplemented with 20% ethylene glycol before flash-freezing with liquid nitrogen. Diffraction data were collected at the Shanghai Synchrotron Radiation Facility (Shanghai, China) beamline BL19U1 under a wavelength of 0.97776 Å, and processed with the HKL 2000 suite[37]. Phase determination by the single wavelength anomalous dispersion (SAD) method and automatic model building were performed in PHENIX[38]. The rest of the model was manually built with Coot[39]. The structure of GSDMA3 was refined in PHENIX, and manual modelling was performed between refinement cycles. The statistics of data collection and refinement are summarized in Extended Data Table 1.The quality of the final model was validated by MolProbity[40]. Ramachandran statistics indicated that all the residues are in the allowed region, in which 97.25% fell into the favoured region. Each asymmetric unit contains one GSDMA3 molecule and the model covers residues 1–453 of the 464 total residues. As well as the C-terminal tail being absent, four loops (residues 66–80, 170–178, 188–193 and 249–263) could not be modelled owing to the lack of interpretable electron density for these highly flexible loops.

Homology-based modelling of GSDMD structure was performed with the program Modeller[41] based on the sequence alignment of GSDMA3 and GSDMD. The structural model of GSDMA3 was completed by using Loop Refine in Modeller and used as the modelling template. The top hit of GSDMD models was evaluated using the DOPE statistical potential score[42] and chosen for subsequent analysis and comparison with GSDMA3 structure. All structural figures were generated in PyMOL (http://www.pymol.org).

31. Zhao, Y. *et al.* The NLRC4 inflammasome receptors for bacterial flagellin and type III secretion apparatus. *Nature* **477,** 596–600 (2011).
32. Gong, Y.-N. *et al.* Chemical probing reveals insights into the signaling mechanism of inflammasome activation. *Cell Res.* **20,** 1289–1305 (2010).
33. Wilschut, J. & Papahadjopoulos, D. Ca^{2+}-induced fusion of phospholipid vesicles monitored by mixing of aqueous contents. *Nature* **281,** 690–692 (1979).
34. Tang, G. *et al.* EMAN2: an extensible image processing suite for electron microscopy. *J. Struct. Biol.* **157,** 38–46 (2007).
35. Scheres, S. H. A Bayesian view on cryo-EM structure determination. *J. Mol. Biol.* **415,** 406–418 (2012).
36. Frank, J. *et al.* SPIDER and WEB: processing and visualization of images in 3D electron microscopy and related fields. *J. Struct. Biol.* **116,** 190–199 (1996).
37. Otwinowski, Z. & Minor, W. in *Methods in Enzymology* Vol. 276 (eds Carter, C. W. Jr & Sweet, R. M.) 307–326 (Academic, 1997).
38. Adams, P. D. *et al.* PHENIX: a comprehensive Python-based system for macromolecular structure solution. *Acta Crystallogr. D* **66,** 213–221 (2010).
39. Emsley, P., Lohkamp, B., Scott, W. G. & Cowtan, K. Features and development of Coot. *Acta Crystallogr. D* **66,** 486–501 (2010).
40. Chen, V. B. *et al.* MolProbity: all-atom structure validation for macromolecular crystallography. *Acta Crystallogr. D* **66,** 12–21 (2010).
41. Eswar, N. *et al.* Comparative protein structure modeling using MODELLER. *Curr. Protoc. Protein Sci.* Chapter 2, Unit 2.9 (2007).
42. Shen, M. Y. & Sali, A. Statistical potential for assessment and prediction of protein structures. *Protein Sci.* **15,** 2507–2524 (2006).

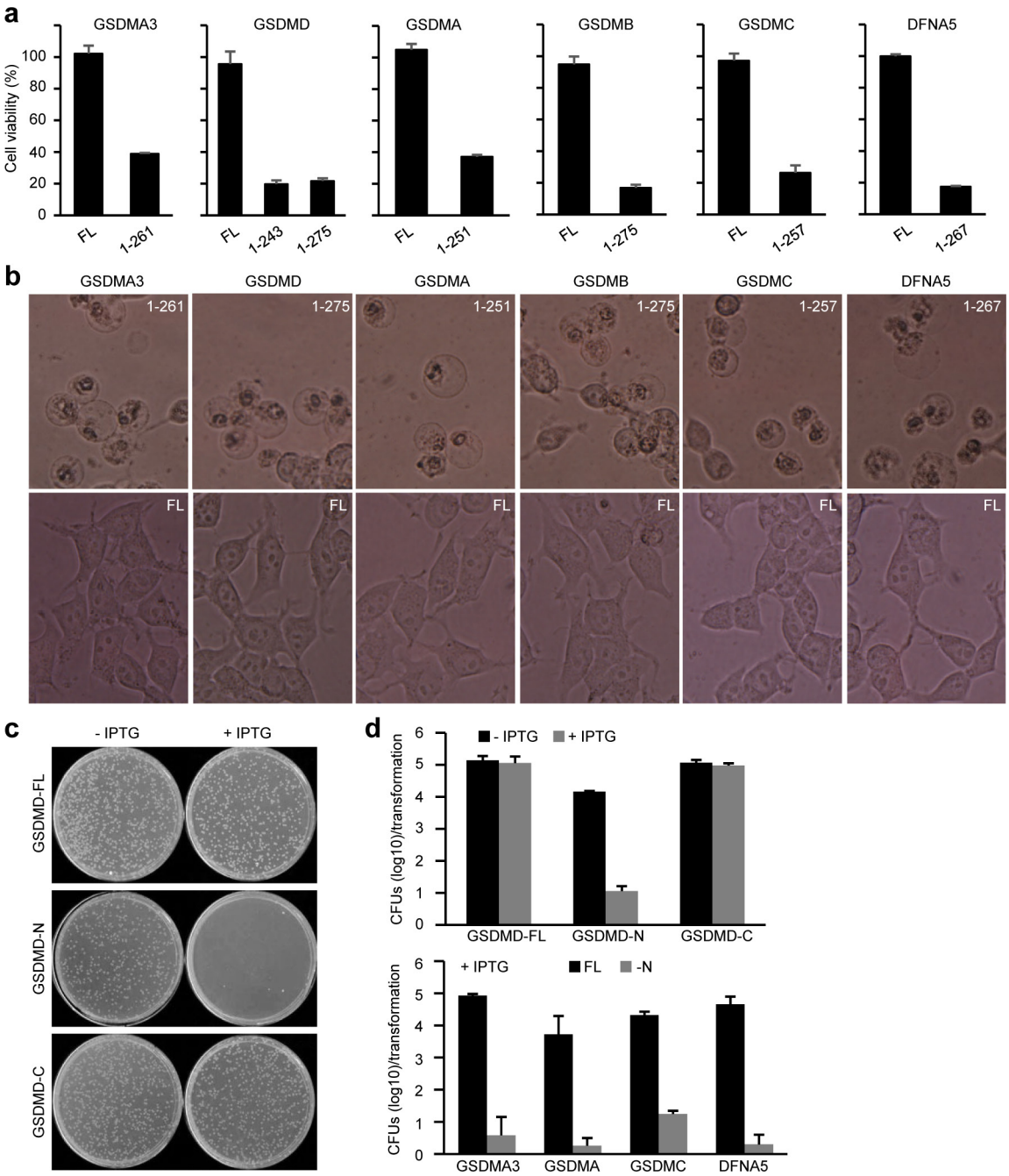

Extended Data Figure 1 | Multiple gasdermin-N domains can induce mammalian cell pyroptosis and also exhibit cytotoxicity in bacteria. **a**, **b**, Full-length (FL) or N-terminal domain regions of different gasdermin-family members were transfected into 293T cells for 20 h. Human GSDMD and mouse GSDMA3 had an N-terminal 3 × Flag tag and human GSDMA, GSDMB, GSDMC and DFNA5 had a C-terminal Flag tag. ATP-based cell viability is expressed as mean ± s.d. from three technical replicates (**a**). Representative views of cell death morphology are shown in **b**. **c**, **d**, Cytotoxicity of the gasdermin-N domain in bacteria. Indicated gasdermins were cloned into an IPTG-inducible vector for transformation into *E. coli*. **c**, Representative agar plates showing transformed *E. coli* colonies for GSDMD. **d**, Bacterial colony-forming units (CFU) per transformation for GSDMD and other gasdermins are shown in the logarithmic form ($\log_{10}$) as mean ± s.d. from three technical replicates. All data shown are representative of three independent experiments.

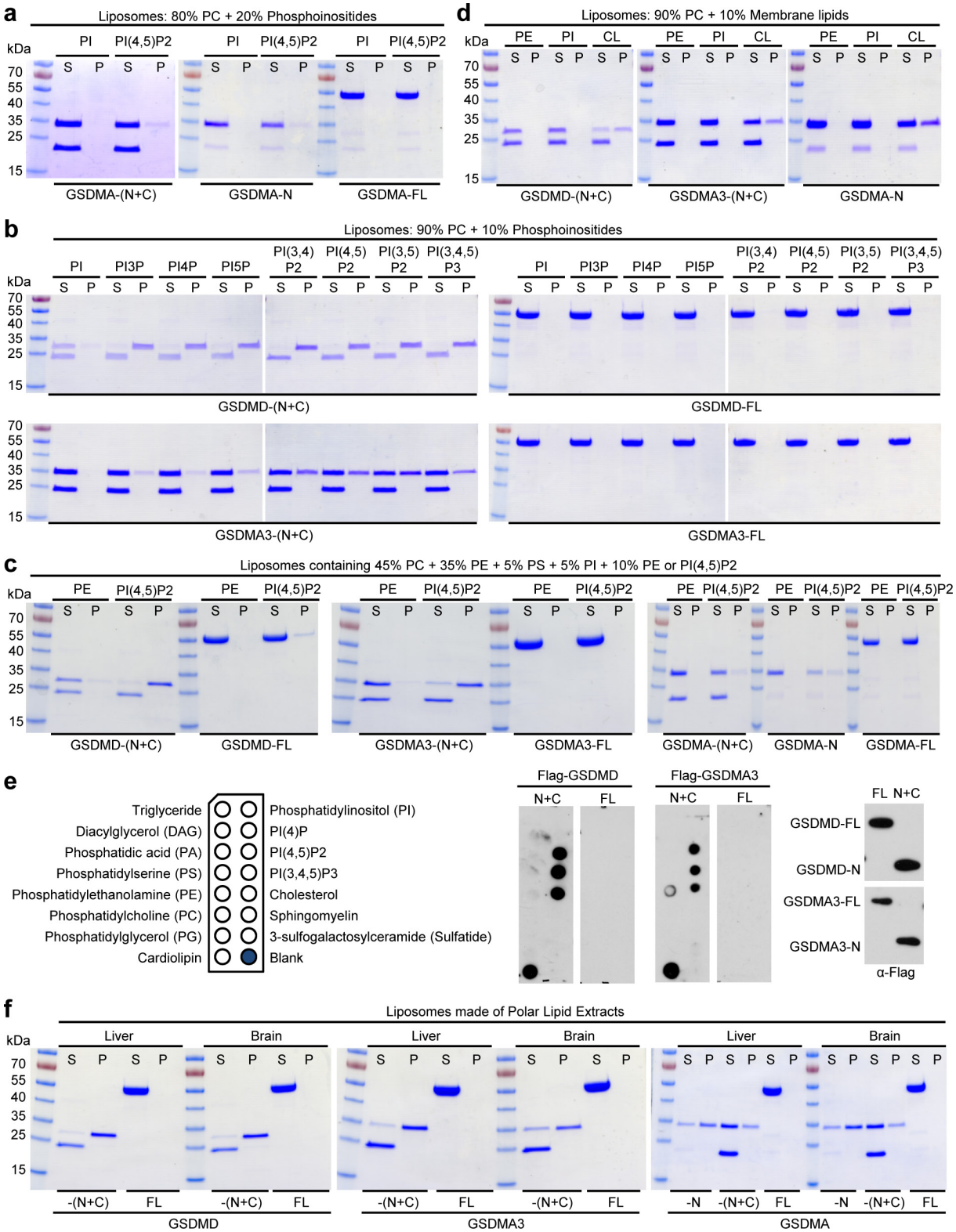

Extended Data Figure 2 | Membrane phospholipid binding of the gasdermin-N domain. a–d, f, Liposomes with indicated lipid compositions (**a–d**) or prepared using bovine liver or brain-derived polar lipid extracts (**f**) were incubated with purified gasdermin proteins. After ultracentrifugation, the liposome-free supernatant (S) and liposome pellet (P) were analysed by SDS–PAGE and Coomassie blue staining. **e**, Noncovalent complex of cleaved GSDMD and GSDMA3 with a Flag tag attached to the end of the gasdermin-N domain or the corresponding uncleaved full-length proteins were incubated with the lipid strips, and the strips were then probed with the anti-Flag antibody. Right, protein loading control. All data shown are representative of three independent experiments.

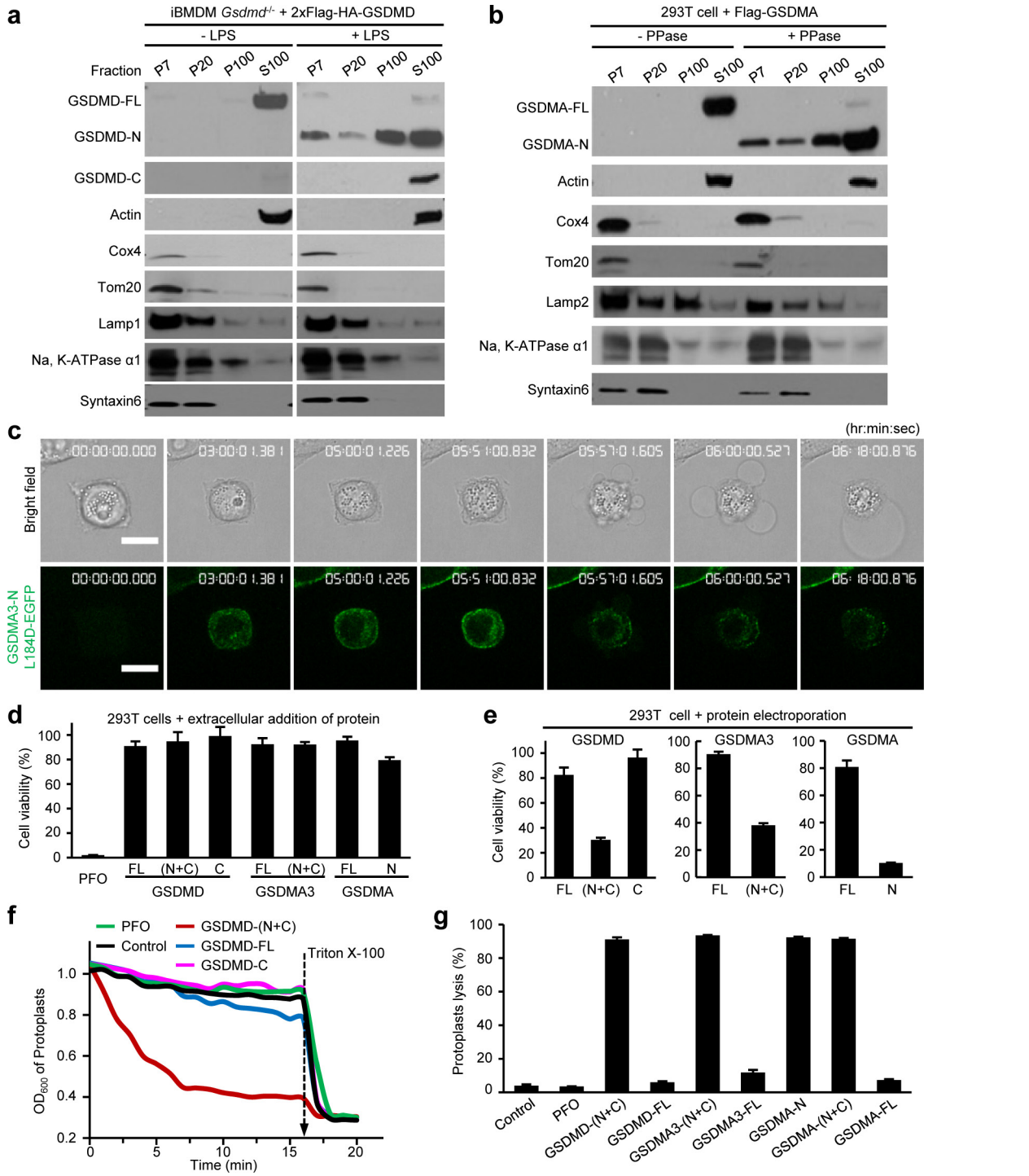

Extended Data Figure 3 | Biomembrane association and lysis by the gasdermin-N domain. a, **b**, Subcellular fractionation of the gasdermin-N domains of GSDMD and GSDMA during pyroptosis. *Gsdmd*$^{-/-}$ iBMDMs expressing 2 × Flag and haemagglutinin (HA)-tagged GSDMD were untreated or stimulated with LPS electroporation (**a**). 293T cells expressing PPase-cleavable Flag–GSDMA were untreated or electroporated with purified PPase (**b**). Homogenized cell extracts were sequentially centrifuged at 700*g*, 20,000*g* and 100,000*g* to separate membrane fractions (P7, P20 and P100) from the S100 soluble fraction. The factions were immunoblotted as indicated. **c**, Microscopy of GSDMA3-N domain localization in cells undergoing pyroptosis. The gasdermin-N domain of GSDMA3 (GSDMA3-N(L184D)) fused N-terminally to eGFP was stably expressed in HeLa cells under a tetracycline-inducible promoter. Shown are representative time-lapse cell images (brightfield and fluorescence) taken from 4–5 h after doxycycline addition. Scale bar, 15 μm. For videos of two representative cells, see Supplementary Videos 3 and 4. **d**, **e**, Effects of extracellular or intracellular delivery of purified gasdermin proteins on 293T cell viability. Equal amounts of indicated gasdermin proteins or PFO were added directly into cell culture medium (**d**) or electroporated into the cytosol (**e**). ATP-based cell viability is expressed as mean ± s.d. from three technical replicates. **f**, **g**, Bacterial protoplast lysis by purified gasdermin proteins. Protoplasts of *B. megaterium* were treated with indicated gasdermin proteins or PFO. Membrane lysis was assessed by measuring the OD_{600} of the protoplasts. Triton-X 100 treatment was used to achieve 100% lysis of the protoplasts. Time-course measurement of GSDMD treatment is shown in **f**. Relative protoplast lysis by GSDMD and other gasdermins is expressed as mean ± s.d. from three technical replicates (**g**). All data shown are representative of three independent experiments.

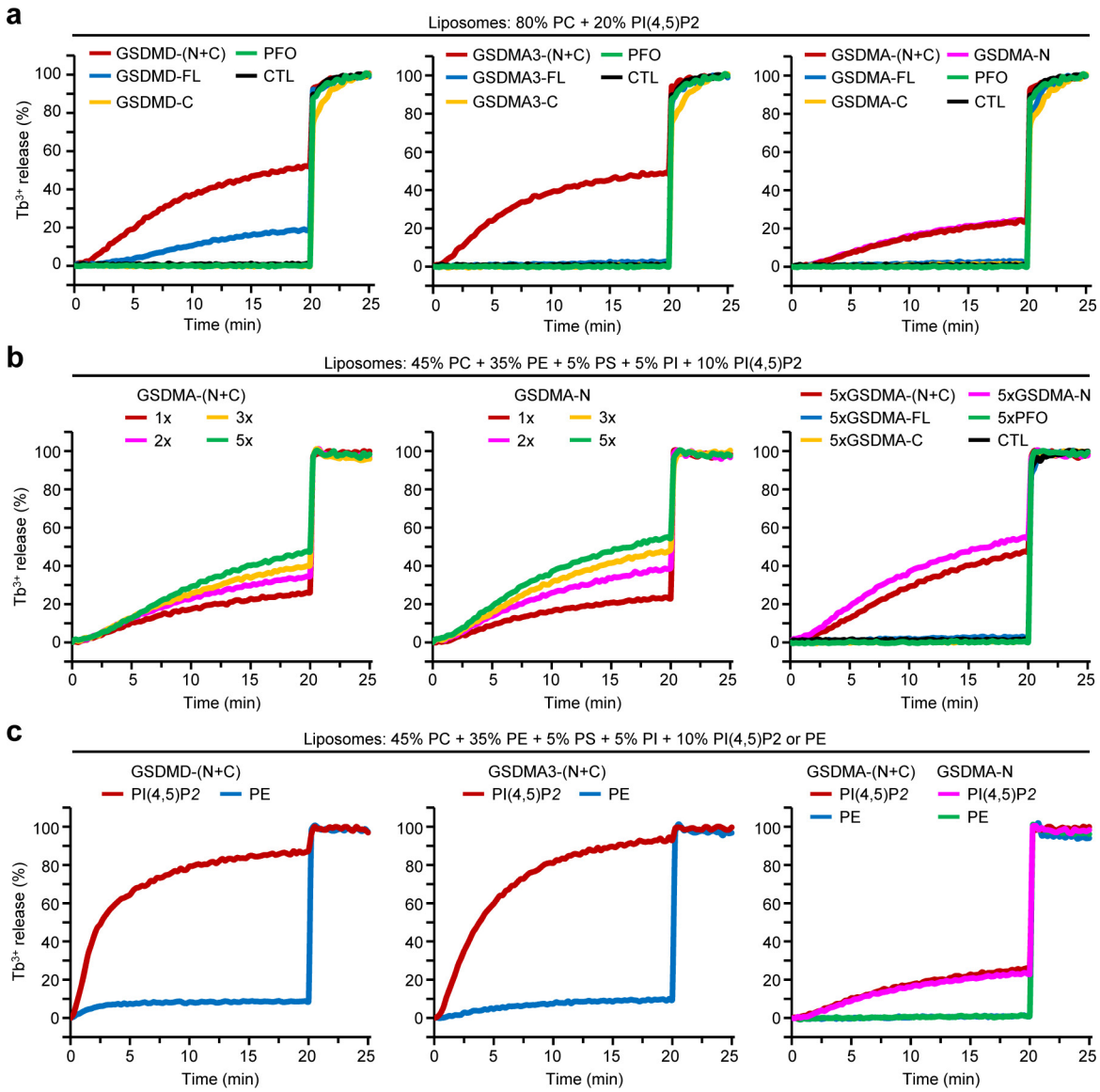

Extended Data Figure 4 | Liposome-leakage-inducing activity of the gasdermin-N domain. a–c, Liposomes with indicated lipid compositions were treated with purified gasdermin proteins or PFO as indicated. Liposome leakage was monitored by measuring DPA chelating-induced fluorescence of released Tb^{3+}. Time course of relative Tb^{3+} release is shown. A dose titration of GSDMA proteins is shown in **b**. CTL, control. All data shown are representative of three independent experiments.

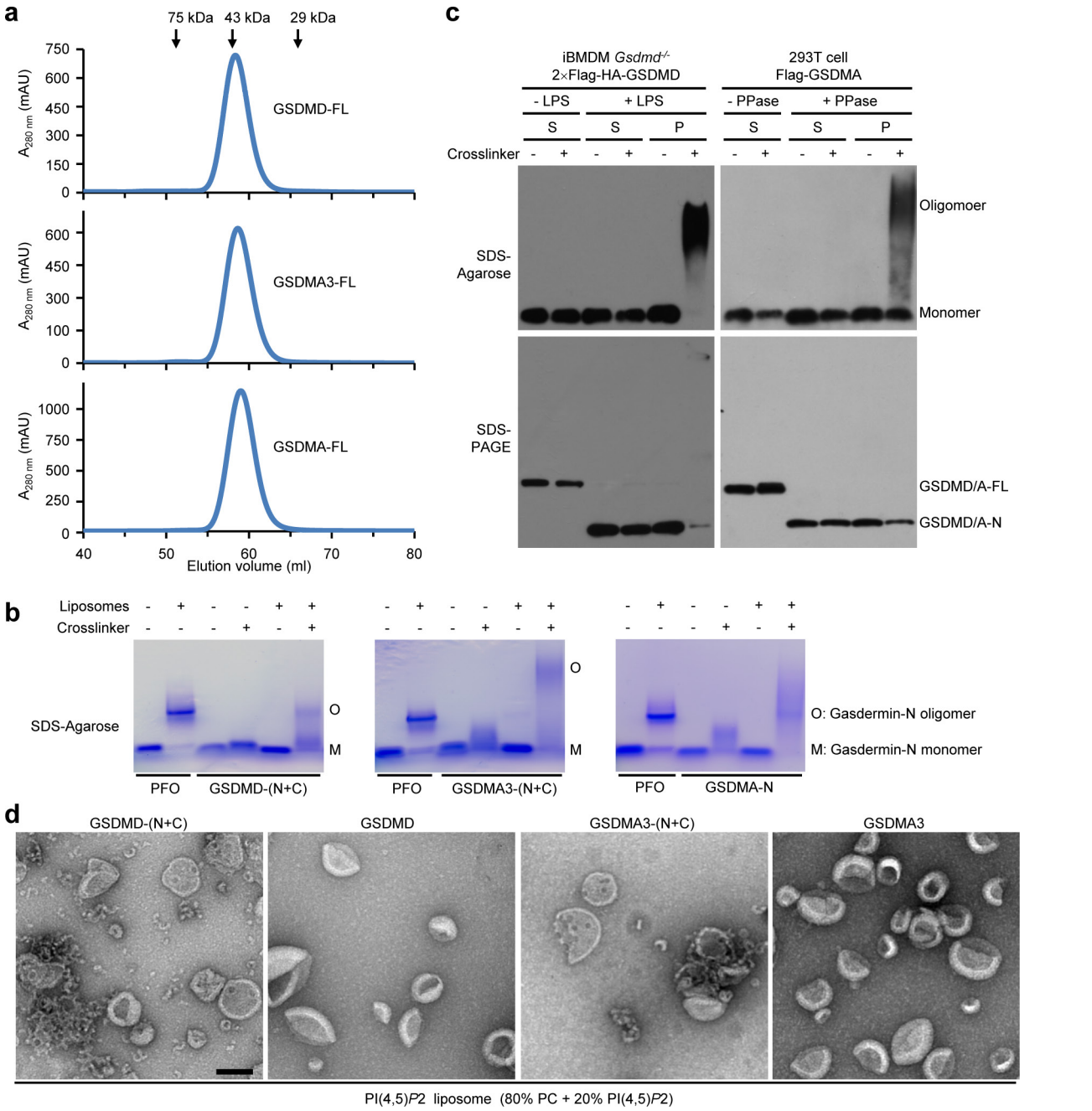

Extended Data Figure 5 | Membrane binding-induced oligomerization of and pore formation by the gasdermin-N domain. a, Gel filtration chromatography of full-length GSDMD, GSDMA and GSDMA3. Indicated gasdermin proteins were loaded on the Superdex G75 column. Arrows indicate elution volume of the molecular mass markers. **b**, Oligomerization of gasdermin-N domain on the liposome membrane. Indicated gasdermin proteins or PFO were incubated with cardiolipin or cholesterol liposomes, respectively. Intact proteins or proteins associated with the liposomes were mock treated or treated with glutaraldehyde and analysed by SDS-agarose gel electrophoresis and Coomassie blue staining. The gasdermin-C domain migrating at the bottom of the gel was omitted for clarity. **c**, Oligomerization of the gasdermin-N domain during pyroptosis. To trigger pyroptosis, *Gsdmd*$^{-/-}$ iBMDMs expressing 2 × Flag-HA–GSDMD and HeLa cells expressing the PPase-cleavable Flag–GSDMA were electroporated with LPS and PPase, respectively. The cytosol (S) and membrane (P) fractions from unstimulated and pyroptotic cells were subjected to glutaraldehyde-mediated crosslinking followed by SDS-agarose (top) or SDS–PAGE (bottom) gel electrophoresis. **d**, Pore-forming activity of the gasdermin-N domain. Liposomes with 80% phosphatidylcholine and 20% PtdIns(4, 5)P_2 were treated with indicated gasdermin proteins. Shown are representative negative-stain electron microscopy micrographs of the liposomes (scale bar, 100 nm). All data shown are representative of three independent experiments.

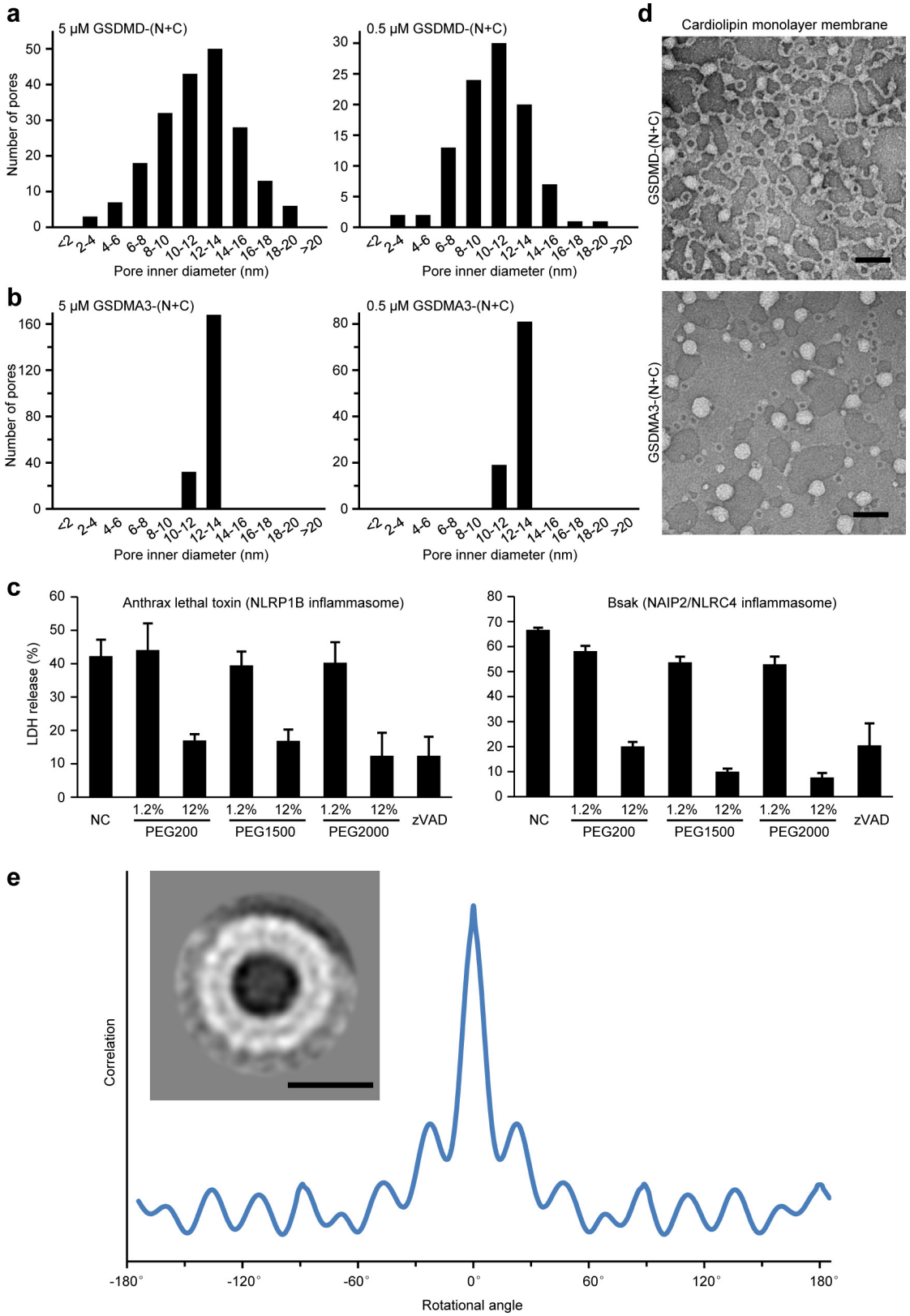

Extended Data Figure 6 | See next page for caption.

Extended Data Figure 6 | Analyses of the gasdermin pore. a, **b**, Size distribution of GSDMD and GSDMA3 pores formed on cardiolipin liposomes. The inner diameters of pores were measured and plotted. A total of 200 or 100 pores for 5 μM or 0.5 μM GSDMD/GSDMA3-treated liposome samples, respectively, were randomly selected from the negative-stain electron microscopy micrographs in Fig. 3a. **c**, Effects of different PEG molecules on lactate dehydrogenase (LDH) release from caspase-1-mediated pyroptotic cells. iBMDMs harbouring a sensitive *Nlrp1b* allele were treated with indicated mass concentration of different PEG molecules and then stimulated with anthrax lethal toxin or LFn-BsaK to activate the canonical NLRP1B or NAIP2/NLRC4 inflammasomes, respectively. 1.2% PEG200 and 12% PEG2000 (mass concentration) have roughly the same molar concentration. Shown are LDH release expressed as mean ± s.d. from three technical replicates. **d**, Pores formed by active GSDMD and GSDMA3 on monolayer membranes containing 80% phosphatidylcholine and 20% cardiolipin. Shown are representative negative-stain electron microscopy micrograph images (scale bar, 100 nm). **e**, Symmetry determination of the gasdermin pore. GSDMA3 pores formed on the monolayer membrane (**d**) were subjected to 2D reference-free classification. One class of pores with the best particle contrast were subjected to rotational auto-correlation calculation and the inlet electron microscopy image (scale bar, 20 nm) shows the averaged view of the class of pores (242 particles). The analyses revealed 16-fold symmetry. Data shown in **a**–**d** are representative of three independent experiments.

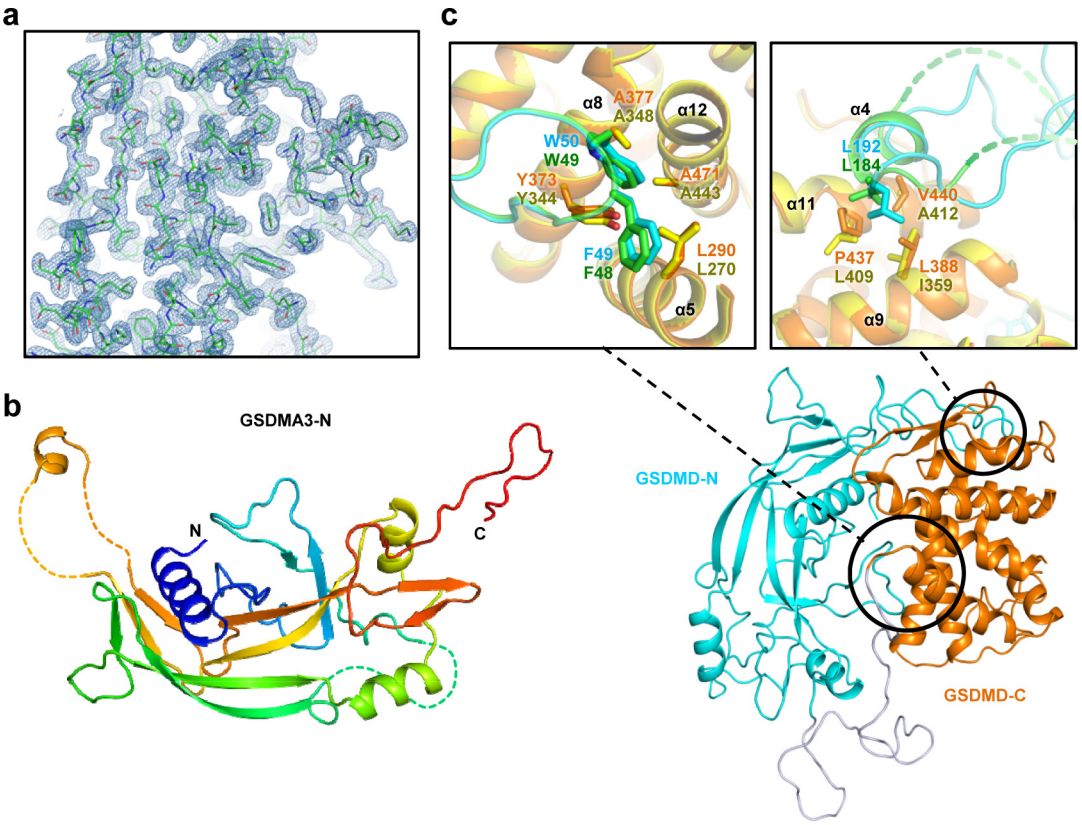

d

No.	PDB chain	Z score	RMSD (Å)	Aligned residues	Identity (%)	Molecule name
1	3hvn-A	5.0	5.4	130	11	Suilysin
2	4cdb-A	4.9	5.4	127	11	Listeriolysin O
3	4qqa-A	4.9	5.9	130	15	Pneumolysin
4	3cqf-A	4.7	5.9	127	10	Anthrolysin O
5	1m3j-A	4.4	5.3	129	12	Perfringolysin O
6	1s3r-A	4.3	5.6	129	11	Intermedilysin
7	3kk7-A	3.4	5.2	116	9	MACPF from *B. thetaiotaomicron*
8	2qp2-A	3.3	5.4	117	11	MACPFfrom *P. luminescens*
9	4wvm-B	3.2	3.4	84	4	Stonustoxin subunit beta
10	4wvm-A	3.1	3.2	85	11	Stonustoxin subunit alpha
11	2qqh-A	3.1	5.1	115	5	Complement component C8 alpha chain
12	3nsj-A	3.0	4.9	111	8	Perforin-1
13	3ojy-B	2.9	5.2	118	8	Complement component C8 beta chain
14	4ov8-A	2.8	6.6	110	4	Pleurotolysin B
15	4e0s-B	2.7	4.9	114	11	Complement component C6

Extended Data Figure 7 | Crystal structure of GSDMA3 and Dali search results for its gasdermin-N domain. a, $2F_o - F_c$ electron density map (contoured at 1.0σ) of GSDMA3 gasdermin-N domain (GSDMA3-N) structure. **b**, Cartoon diagram of GSDMA3-N structure. **c**, Structural model of GSDMD obtained from homology modelling and the conserved autoinhibitory interactions. Bottom, overall structure of modelled GSDMD; top, comparisons of the hydrophobic core (left) and the second inter-domain contact (right) with the corresponding structures in GSDMA3. Conserved residues involved in the autoinhibitory interactions are labelled and shown as sticks. Cyan, GSDMD-N; orange, GSDMD-C; green, GSDMA3-N; yellow, GSDMA3-C. **d**, Dali search results for the GSDMA3-N structure.

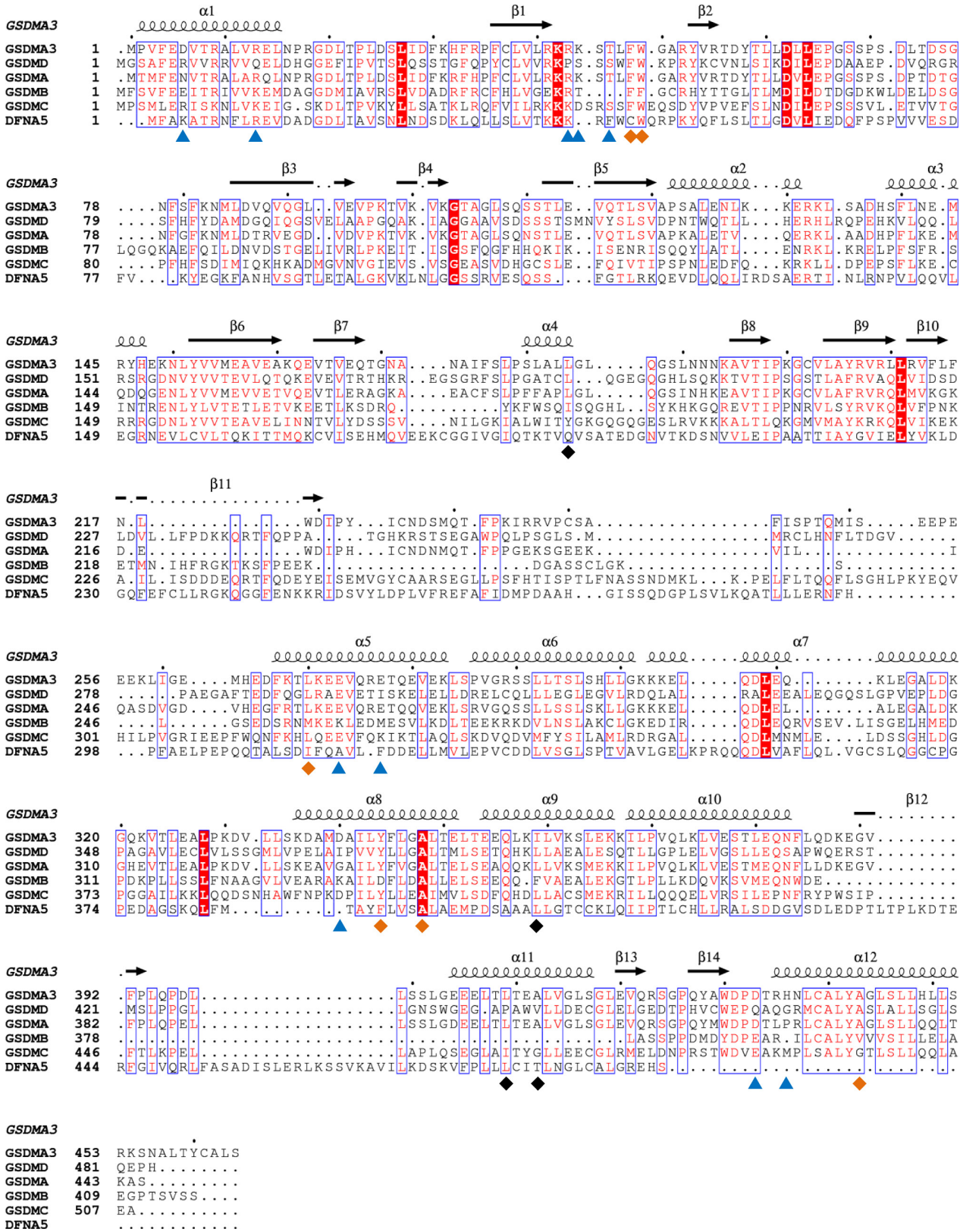

Extended Data Figure 8 | Multiple sequence alignment of gasdermin family members. GSDMA3 is a mouse protein and sequences of other gasdermins are from human. The secondary structures determined from GSDMA3 are marked along the sequence. The alignment was performed with the ClustalW2 algorithm with structure-based manual adjustment of the α4 region in GSDMA3 and GSDMD. Identical residues are highlighted by dark red background and conserved residues are coloured red. The residues involved in the autoinhibitory interactions are marked underneath the sequences with blue triangle for polar residues, orange rhombus for hydrophobic residues and black rhombus for hydrophobic residues in the second inter-domain interface. The residue number is indicated on the left of the sequence.

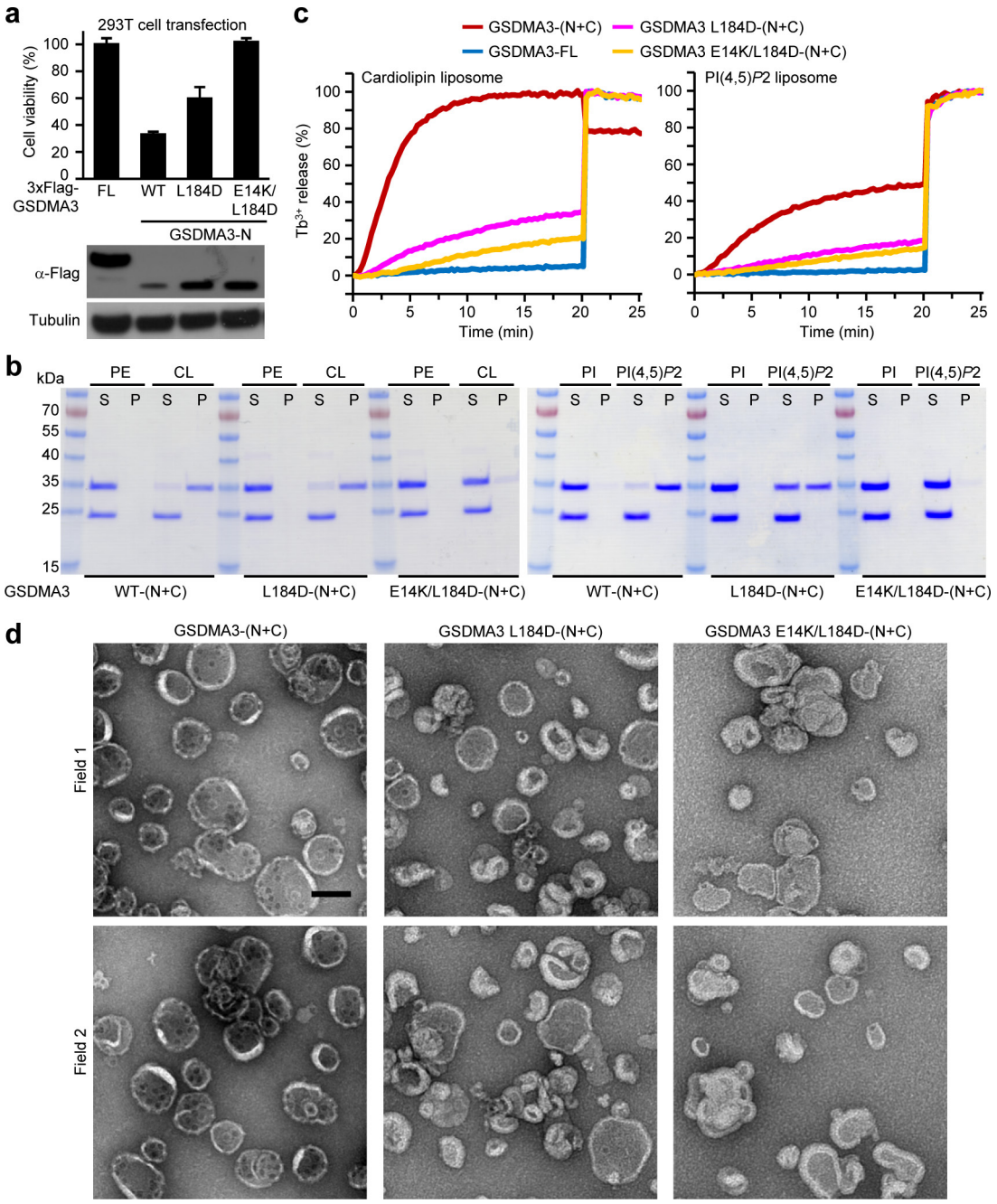

Extended Data Figure 9 | Mutations in GSDMA3-N affecting lipid binding and pore formation also reduce pyroptosis. a, Effects of L184D/E14K mutations on pyroptosis-inducing activity of GSDMA3-N (residues 1–284). Full-length GSDMA3 or its gasdermin-N domain (wild type or indicated mutants) was transfected into 293T cells. ATP-based cell viability is expressed as mean ± s.d. from three technical replicates. **b**, **c**, Effects of L184D/E14K mutations on lipid-binding and liposome-leakage-inducing activities of GSDMA3-N domain. Liposomes containing 80% phosphatidylcholine and 20% phosphatidylethanolamine, cardiolipin, phosphatidylinositol or PtdIns(4,5)P_2 were treated with purified GSDMA3. After ultracentrifugation, the liposome-free supernatant (S) and the liposome pellet (P) were analysed by SDS–PAGE (**b**). Liposome leakage was monitored by measuring DPA chelating-induced fluorescence of released Tb^{3+} (**c**). Triton-X 100 treatment was used to achieve 100% leakage. **d**, Effects of L184D/E14K mutations on pore formation by GSDMA3-N. Representative electron microscopy images of the pores on the cardiolipin liposome are shown (scale bar, 100 nm). All data shown are representative of three independent experiments.

Extended Data Table 1 | Data collection refinement statistics

	Se_GSDMA3(1-464) (5B5R)
Data collection	
Space group	$P2_1$
Cell dimensions	
a, *b*, *c* (Å)	43.453, 103.414, 49.625
α, β, γ (°)	90.00, 110.57, 90.00
Wavelength (Å)	0.97776
Resolution (Å)[a]	50.00-1.90 (1.93-1.90)[a]
R_{merge}	0.071 (0.876)
$I/\sigma(I)$	25.6 (2.4)
Completeness (%)	97.1 (92.7)
Redundancy	6.6 (5.1)
Refinement	
Resolution (Å)	37.91-1.90
No. reflections	44,110
R_{work} / R_{free}	0.1892/0.2319
No. atoms	
Protein	3,264
Water	218
B factors	
Protein	28.36
Water	33.91
r.m.s deviations	
Bond lengths (Å)	0.005
Bond angles (°)	0.848

One SeMet crystal was used for data collection and structure determination.
*Values in parentheses are for highest-resolution shell.